Electronic Supplementary Material (ESI) for Journal of Materials Chemistry A.

SI

Fine-tuning optimal porous coordination polymers by functional alkyl groups for CH_4 purification

Fujun Cheng[a]†, Qianqian Li[a]†, Jingui Duan[a,e*], Nobuhiko Hosono[b], Shin-ichiro Noro[c], Rajamani Krishna[d], Hongliang Lyu[a], Shinpei Kusaka[b], Wanqin Jin[a*] and Susumu Kitagawa[b*]

[a] State Key Laboratory of Materials-Oriented Chemical Engineering, College of Chemical Engineering, Nanjing Tech University, Nanjing 210009, China. *Email: duanjingui@njtech.edu.cn; wqjin@ njtech.edu.cn

[b] Institute for Integrated Cell-Material Sciences, Kyoto University, Yoshida, Sakyo-ku, Kyoto 606-8501, Japan. *Email: kitagawa@icems.kyoto-u.ac.jp.

[c] Research Institute for Electronic Science, Hokkaido University, Sapporo 001-0020, Japan.

[d] Van 't Hoff Institute for Molecular Sciences, University of Amsterdam, Science Park 904, 1098 XH Amsterdam, The Netherlands.

[e] Jiangsu National Synergetic Innovation Center for Advanced Materials, Nanjing Tech University, Nanjing, 210009, China.

General Procedures and Materials

All air-sensitive reactions were carried out under a dry nitrogen atmosphere using standard Schlenk techniques. All the reagents and solvents were commercially available and used as received. The FTIR spectra were recorded in the range of 4000-500 cm^{-1} on a Nicolet ID5 ATR spectrometer. Thermal analyses were performed on a Universal V3.9A TA Instruments from room temperature to 700°C with a heating rate of 10°C/min under flowing nitrogen. ^{1}H and ^{13}C NMR spectra were recorded on a Bruker 600 FT-NMR spectrometer. The powder X-ray diffraction patterns (PXRD) measurements were carried on a Bruker axs D8 Advance 40kV, 40mA for CuK_{α} (θ= 1.5418 Å) with a scan rate of 0.2 s/deg at room temperature. X-ray thermodiffractometry of as-synthesized PCPs were performed under an N_2 atmosphere from room temperature to 350℃. Simulated powder patterns from single-crystal X-ray diffraction data were generated using Mercury 1.4.2 software.

Ligand synthesis

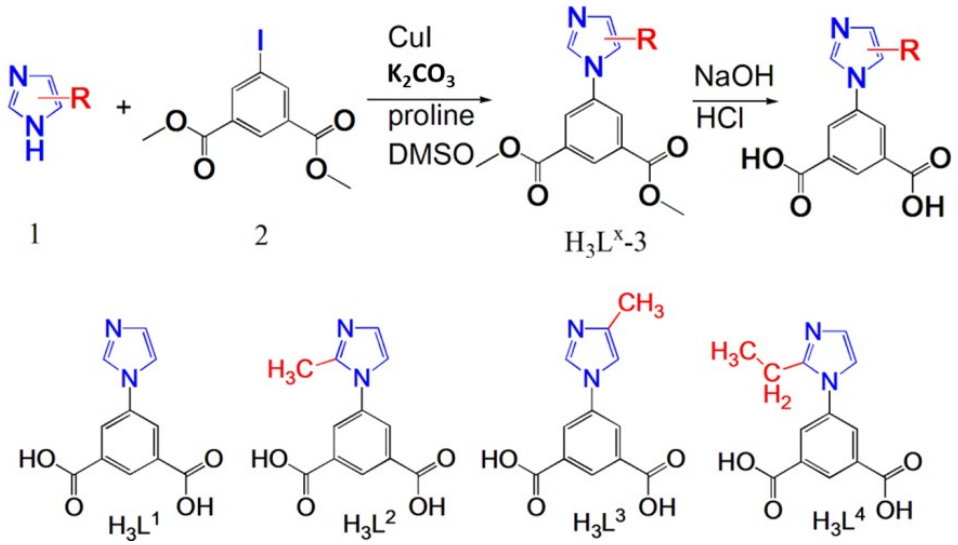

Synthesis of Compound (H_3L^1-3 Methyl ester)

Same experiment conditions, except corresponded imidazole derivatives, were used for ligands syntheses. Thus, we just describe the detail of H_3L^1 synthesis.

5-Iodo-

isophthalic acid dimethyl ester (3.6 g, 11.4 mmol), excess of imidazole (1.55 g,22.8 mmol), K_2CO_3 (3.14g,22.8mmol), CuI (0.44g 2.28mmol) and proline (0.52 g, 4.56 mmol, 0.4 equi v) were combined in dry DMSO (70 mL). The reaction system was bubbled by N_2 for 30 mins and subsequent heating at reflux for 24 hours. After the temperature cooling down, the reaction mixture was filtered. The filtrate was extracted by adding water (70 mL) and EtOAc (100 ×3 mL), dried over anhydrous $MgSO_4$, filtrated, and then concentrated. The residue was purified by silica gel column chromatography using EtOAC/Hexane (from 1:1 to 9:1) to give **H_3L^1-3** as a white solid in 62 % yield (4.80 g, 11.8 mmol).

^{1}H NMR ($CDCl_3$) of **H_3L^1-3**: 8.36 (s, 1H), 8.30 (s, 2H), 7.92 (s, 1H), 7.48 (s, 1H), 7.21 (s, 1H), 3.98 (s, 6H). ^{13}C NMR (CDCl3) of **H_3L^1-3**: 166.11, 138.83, 138.35, 136.45, 131.54, 127.72, 125.20, 118.22, 53.52.

^{1}H NMR ($CDCl_3$) of **H_3L^2-3**: 8.73 (s, 1H), 8.34 (s, 1H), 8.31 (s, 2H), 7.63 (s, 1H), 3.99 (s, 6H), 2.12 (s, 3H). ^{13}C NMR (CDCl3) of **H_3L^2-3**: 165.08, 139.69, 138.44, 136.21, 132.88, 127.79, 125.09, 115.02, 52.88, 10.66.

^{1}H NMR ($CDCl_3$) of **H_3L^3-3**: 8.36 (s, 1H), 8.36 (s, 1H), 8.34 (s, 1H), 8.31 (s, 2H), 7.63 (s, 1H), 3.97 (s, 6H), 2.42 (s, 3H). ^{13}C NMR (CDCl3) of **H_3L^2-3**: 165.05, 139.74, 138.56, 136.01, 132.95, 127.64, 125.22, 115.12, 52.37, 14.86.

^{1}H NMR ($CDCl_3$) of **H_3L^4-3**: 8.72 (s, 1H), 8.14 (s, 1H), 7.10 (s, 1H), 7.02 (s, 2H), 3.97 (s, 6H), 2.62 (q, 2H), 1.26 (t, 3H). ^{13}C NMR (CDCl3) of **H_3L^4-3**: 165.05, 149.57, 138.42, 132.27, 130.65, 130.18, 128.11, 120.46, 52.77, 20.58, 12.20.

Synthesis of H_3L^1

H_3L^1-3 (0.7 g, 2.6 mmol) was dissolved in THF (15 mL) and MeOH (15 mL). A solution of NaOH (2.1 g, 52 mmol, 20 equiv) in H_2O (30 mL) was added and the suspension heated at reflux for 10 hours upon which a clear solution was achieved. The organic solvents were evaporated and HCl (conc.) was added dropwise with stirring, precipitating the product. The flask was cooled to 0°C to ensure complete precipitation, the solids collected by filtration, washed thoroughly with water and dried at 80°C to give the desired product **H_3L^1** (0.6 g) as a white solid.

^{1}H NMR (DMSO) of **H_3L^1**: 13.61 (br s, 1.4H), 8.45 (s, 1H), 8.41 (s, 1H), 8.34 (s, 2H), 7.94 (s, 1H), 7.15 (s, 1H). ^{13}C NMR (DMSO) of **H_3L^1**: 166.36, 138.02, 136.46, 133.58, 130.71, 128.34, 125.51, 118.80.

^{1}H NMR (DMSO) of **H_3L^2**: 13.55 (br s, 0.5H), 8.56 (s, 1H), 8.25 (s, 2H), 7.73 (s, 1H), 7.41 (s, 1H), 2.43 (s, 3H). ^{13}C NMR (DMSO) of **H_3L^2**: 166.10, 145.16, 137.09, 133.57, 130.76, 130.57, 122.97, 122.57, 12.72.

^{1}H NMR (DMSO) of **H_3L^3**: 8.39 (s, 1H), 8.33 (s, 1H), 8.27 (s, 2H), 7.62 (s, 1H), 2.12 (s, 3H). ^{13}C NMR (DMSO) of **H_3L^3**: 166.65, 139.42, 138.18, 135.79, 133.96, 128.22, 124.89, 115.08, 14.15.
^{1}H NMR (DMSO) of **H_3L^4**: 8.63 (s, 1H), 8.38 (s, 2H), 7.94 (s, 1H), 7.78 (s, 1H), 2.84 (q, 2H), 1.24 (t, 3H). ^{13}C NMR (DMSO) of **H_3L^4**: 165.35, 149.11, 135.37, 133.11, 131.03, 123.09, 118.87, 55.97, 18.58, 10.80.

Single crystal X-ray studies

Single-crystal X-ray diffraction data were measured on a Bruker Smart Apex CCD diffractometer at 298 K using graphite monochromated Mo/Kα radiation (λ = 0.71073 Å). Data reduction was made with the Bruker Saint program. The cryst$_a$l of NJU-Bai3 was mounted in a flame sealed capillary containing a small amount of mother liquor to prevent desolvation during data collection, and data were collected at 298K. The structure was solved by direct methods and refined using the full-matrix least squares technique using the SHELXTL package[1]. Nonhydrogen atoms were refined with anisotropic displacement parameters during the final cycles. Organic hydrogen atoms were placed in calculated positions with isotropic displacement parameters set to 1.2Ueq of the attached atom. The unit cell includes a large region of disordered solvent molecules, which could not be modeled as discrete atomic sites. We employed PLATON/SQUEEZE[2,3] to calculate the diffraction contribution of the solvent molecules and, thereby, to produce a set of solvent-free diffraction intensities; the structure was then refined again using the data generated.

Table S1. Crystal data and structure refinement for **NTU-11** to **-14** at 298 K.

	NTU-11	**NTU-12**	**NTU-13**	**NTU-14**
Empirical formula	$C_{11}H_6CuN_2O_4$	$C_{12}H_8CuN_2O_4$	$C_{12}H_8CuN_2O_4$	$C_{13}H_{10}CuN_2O_4$
Formula weight	293.73	307.75	307.75	321.78
Crystal system	monoclinic	orthorhombic	monoclinic	monoclinic
Space group	*P21/c*	*Pbcn*	*P21/c*	*P21/c*
Unit cell dimensions	*a* = 10.830(7)Å *b* = 11.889(8)Å *c* = 14.559(9)Å *β* = 109.594(8)°	*a*= 12.678(5)Å *b*= 14.408(5)Å *c*= 20.225(7)Å	*a*= 10.915(10)Å *b*= 11.321(10)Å *c*= 14.814(12)Å *β*=109.602(13)°	*a*= 10.93(3)Å *b*= 13.71(4)Å *c*= 13.47(3)Å *β*= 111.86(3)°
Volume	1766(2) $Å^3$	3694(2) $Å^3$	1725(3) $Å^3$	1873(9) $Å^3$
Z	4	8	4	4
Density (calculated)	1.105 g/cm^3	1.107 g/cm^3	1.185 g/cm^3	1.141 g/cm^3
Mu(MoKa)	1.241 mm^{-1}	1.189 mm^{-1}	1.274 mm^{-1}	1.176 mm^{-1}
$F_{(000)}$	588	1240	620	652
Theta min-max	2.0, 25.0	2.0, 23.1	2.0, 25.0	2.2, 26.0
Index ranges	-12<=h<=12 -14<=k<=14 -16<=l<=17	-14<=h<=13 -15<=k<=15 -22<=l<=22	-11<=h<=13 -13<=k<=13 -17<=l<=17	-11<=h<=13 -16<=k<=16 -16<=l<=16
Tot., Uniq. Data, R(int)	9851,2672, 0.098	20783,2618, 0.229	11191,3042, 0.070	12914,3597, 0.154
Observed data [I > 2σ (I)]	1627	1463	2147	1575
*N*ref, *N*par	2672, 163	2618, 173	3042, 173	3597, 173
R_1, wR_2, S	0.0899, 0.2592, 1.01	0.1032, 0.2639, 1.00	0.0990, 0.3160, 1.17	0.1123, 0.3116, 1.00
Max Shift	0	0	0	0

$R = \Sigma||F_o|-|F_c||/\Sigma|F_o|$, $wR = \{\Sigma[w(|F_o|^2 - |F_c|^2)^2]/\Sigma[w(|F_o|^4)]\}^{1/2}$ and $w = 1/[\sigma^2(F_o^2) + (0.1452P)^2]$ where $P = (F_o^2+2F_c^2)/3$

Adsorption Experiments. Before the measurement, the solvent-exchanged sample was prepared by immersing the as-synthesized samples in dehydrated methanol for two days to remove the nonvolatile solvents, and the extract was decanted every 8 h and fresh acetone was replaced. The completely activated sample was obtained by heating the solvent-exchanged sample at room temperature for 6 h, 60°C for 6 h and then120°C for 24h under a dynamic high vacuum. In the gas sorption measurement, ultra-high-purity grade were used throughout the adsorption experiments. N_2 of the measured sorption isotherms have been repeated twice to confirm the reproducibility within experimental error. Gas adsorption isotherms were obtained using a Belsorpvolumetric adsorption instrument from BEL Japan Inc. using the volumetric technique.

Co-sorption measurements. Mix gas adsorptions were carried out using a multicomponent gas adsorption apparatus, Belsorp-VC (MicrotracBEL Corp.). In this apparatus, the total adsorbed amount was calculated by a constant volume method, and the composition ratio of mixed gases was determined using an Agilent 490 Micro gas chromatographic system equipped with a thermal conductive detector. From these data, we calculated adsorbed amounts and partial pressures for each gas.

Water stability experiments

For water and chemical treatment, fresh samples were soaked (around 100 mg for each) into three bottles (10 ml). HCl and NaOH were used to turn the pH of the solution to 2, 7 and 12. After one day treatment, partial samples were used for PXRD patterns collections and partial samples were used for gas sorption experiments (washed by ethanol three times and degassed at 120°C for 24h). In addition, for long term test, **NTU-14** was soaked in water at room temperature for 15 and 60 days.

Fitting of pure component isotherms

The isotherm data for H_2, CH_4, CO, CO_2, C_2H_4, and C_2H_6 in **NTU-12**, **NTU-13**, and **NTU-14** were measured at three different temperatures 273 K, 283 K, and 298 K. The data were fitted with either the single-site Langmuir or the Dual-site Langmuir model. The single-site, or dual-site Langmuir parameters are provided in Table S2, S3, S4, and S5.

$$q = q_{A,sat}\frac{b_A p}{1+b_A p} + q_{B,sat}\frac{b_B p}{1+b_B p} \qquad (1)$$

The Langmuir parameters for each site is temperature-dependent

$$b_A = b_{A0}\exp\left(\frac{E_A}{RT}\right); \quad b_b = b_{B0}\exp\left(\frac{E_B}{RT}\right); \qquad (2)$$

Table S2. *T*-dependent dual-site Langmuir parameters for CH_4, CO, CO_2, C_2H_4, and C_2H_6 in **NTU-12**.

	Site A			Site B		
	$q_{A,sat}$ mol/kg	b_{A0} Pa^{-1}	E_A kJ mol^{-1}	$q_{B,sat}$ mol/kg	b_{B0} Pa^{-1}	E_B kJ mol^{-1}
C_2H_6	4.6	7.29×10^{-12}	33	2.6	8.55×10^{-10}	29.4
C_2H_4	4	2.32×10^{-11}	30	3	3.83×10^{-10}	30
CH_4	4.6	1.36×10^{-9}	19			
CO	0.1	8.00×10^{-7}	17	3.9	1.14×10^{-9}	17
CO_2	9.4	4.85×10^{-11}	29.3	2.6	8.55×10^{-10}	29.4

Table S3. *T*-dependent dual-site Langmuir parameters for CH_4, CO, CO_2, C_2H_4, and C_2H_6 in **NTU-13**.

	Site A			Site B		
	$q_{A,sat}$ mol/kg	b_{A0} Pa^{-1}	E_A kJ mol^{-1}	$q_{B,sat}$ mol/kg	b_{B0} Pa^{-1}	E_B kJ mol^{-1}
C_2H_6	0.8	8.85×10^{-12}	33	3	9.76×10^{-11}	36.7
C_2H_4	0.7	1.96×10^{-11}	31.6	3	7.43×10^{-11}	36.3
CH_4	3	4.61×10^{-10}	24.5			
CO	0.08	7.04×10^{-8}	21.6	4.5	2.33×10^{-10}	21.6
CO_2	3.5	1.64×10^{-11}	30	2.8	7.13×10^{-11}	34.8

Table S4. *T*-dependent dual-site Langmuir parameters for CH_4, CO, CO_2, C_2H_4, and C_2H_6 in **NTU-14**.

	Site A			Site B		
	$q_{A,sat}$ mol/kg	b_{A0} Pa^{-1}	E_A kJ mol^{-1}	$q_{B,sat}$ mol/kg	b_{B0} Pa^{-1}	E_B kJ mol^{-1}
C_2H_6	3.1	2.19×10^{-11}	37.3			
C_2H_4	3.2	5.55×10^{-11}	34.4			

CH_4	3.2	7.24×10^{-10}	21.3			
CO	0.025	1.12×10^{-6}	18.6	2.4	8.58×10^{-10}	18.6
CO_2	4.8	6.34×10^{-11}	30			

Table S5. Langmuir parameters for H_2 at 298 K in **NTU-12**, **NTU-13**, and **NTU-14**.

	$q_{A,sat}$ mol/kg	b_A Pa^{-1}
NTU-12	4	7.91×10^{-8}
NTU-13	5	4.37×10^{-8}
NTU-14	5	6.00×10^{-8}

Isosteric heat of adsorption

The binding energies of CH_4, CO, CO_2, C_2H_4, and C_2H_6 in **NTU-12**, **NTU-13**, and **NTU-14** are reflected in the isosteric heat of adsorption, Q_{st}, defined as

$$Q_{st} = RT^2\left(\frac{\partial \ln p}{\partial T}\right)_q \qquad (3)$$

These values were determined using the pure component isotherm fits.

The adsorption selectivities of the three binary pairs C_2H_4/CH_4, C_2H_4/CO, and C_2H_4/H_2 can be determined from

$$S_{ads} = \frac{q_i/q_j}{p_i/p_j} \qquad (4)$$

In equation (4), q_i, and q_j are the molar loadings in the adsorbed phase in equilibrium with the bulk gas phase with partial pressures p_i, and p_j.

Transient breakthrough of mixtures in fixed bed adsorbers

The performance of industrial fixed bed adsorbers is dictated by a combination of adsorption selectivity and uptake capacity. For a proper comparison of **NTU-12**, **NTU-13**, and **NTU-14**, we perform transient breakthrough simulations using the simulation methodology described in the literature[4-6]. For the breakthrough simulations, the following parameter values were used: length of packed bed, L = 0.3 m; voidage of packed bed, □ = 0.4; superficial gas velocity at inlet, u = 0.04 m/s. The transient breakthrough simulation results are presented in terms of a *dimensionless* time, ε, defined by dividing the actual time, t, by the characteristic time, $\frac{L\varepsilon}{u}$.

Structures of NTU-11 to -14

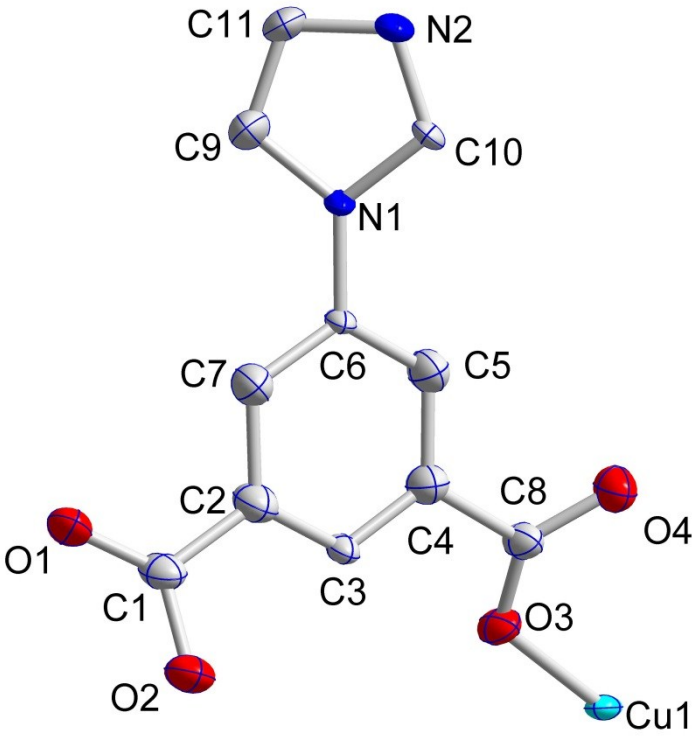

Fig. S1 View of asymmetric unit of **NTU-11**.

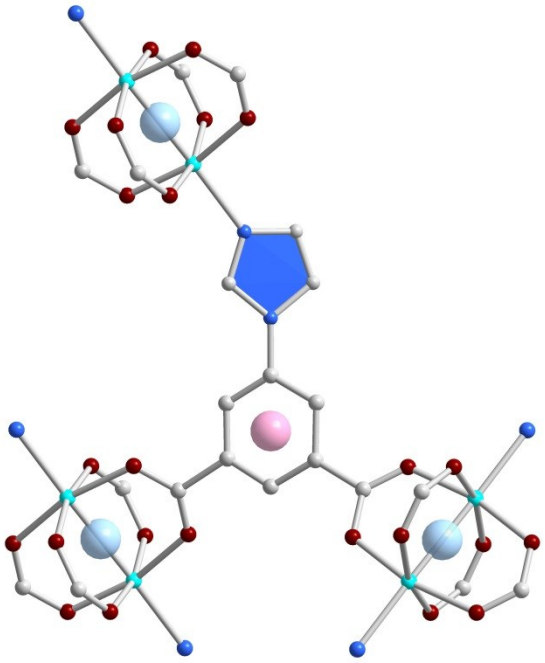

Fig. S2 View of ligand connection of **NTU-11**.

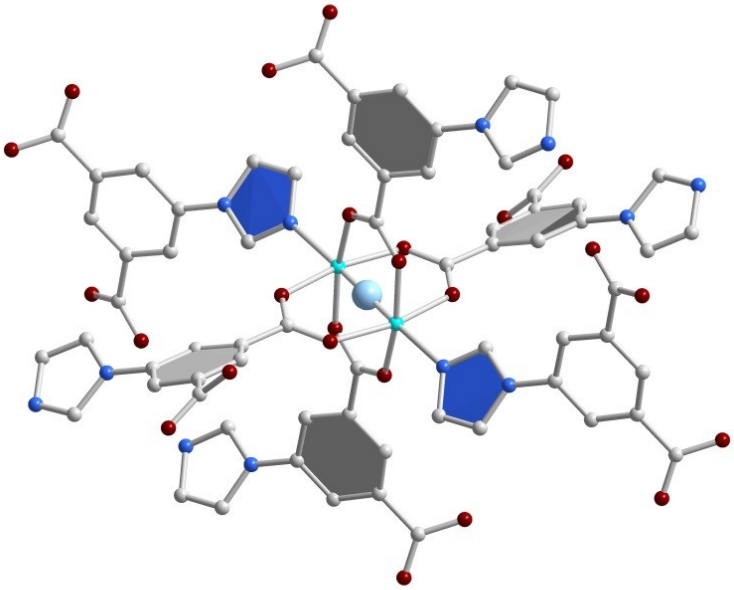

Fig. S3 View of cluster connection of **NTU-11**.

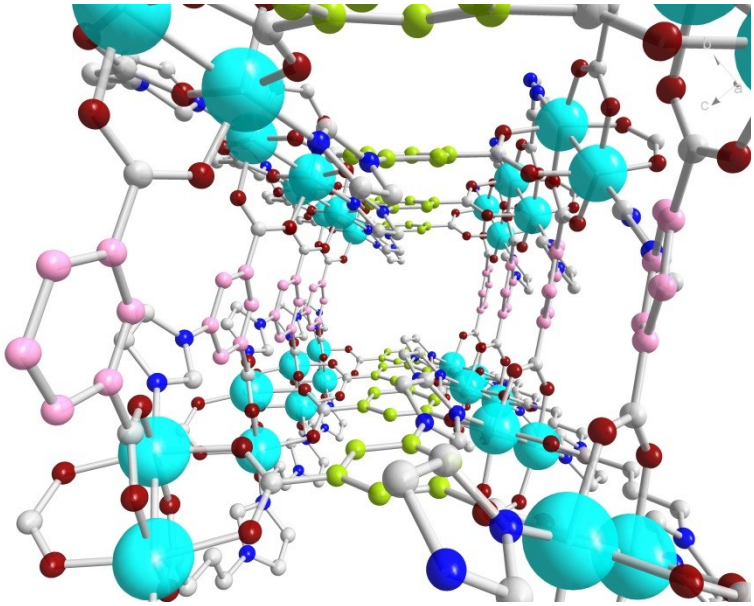

Fig. S4 View of 1D channel in **NTU-11** along c-axis.

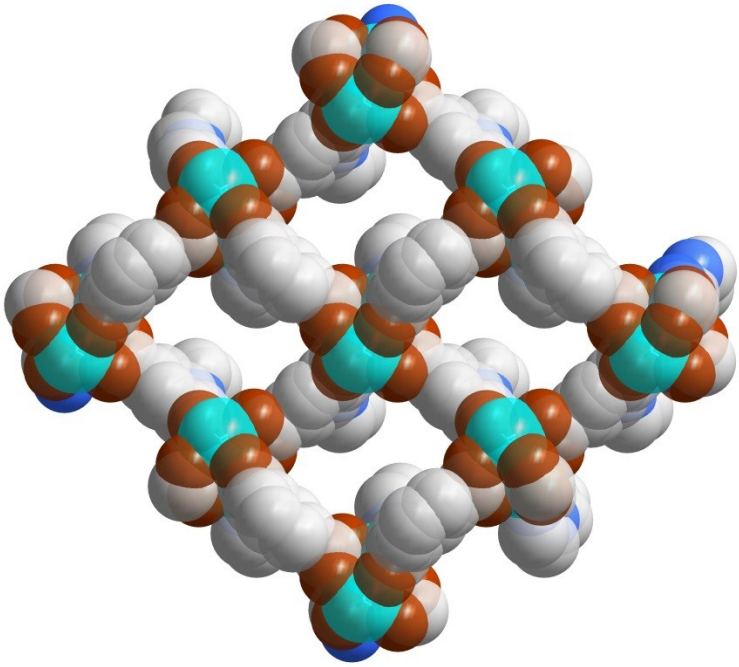

Fig. S5 View of crystal packing along c-axis in **NTU-11**.

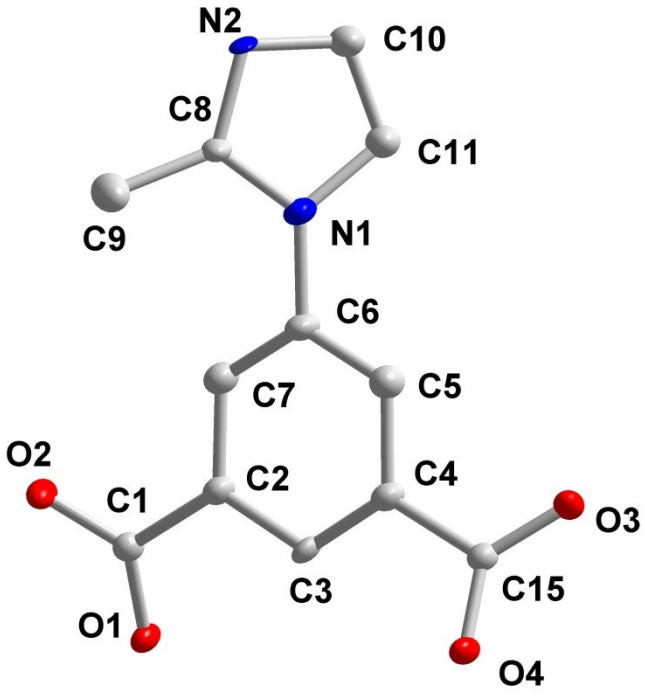

Fig. S6 View of asymmetric unit of **NTU-12**.

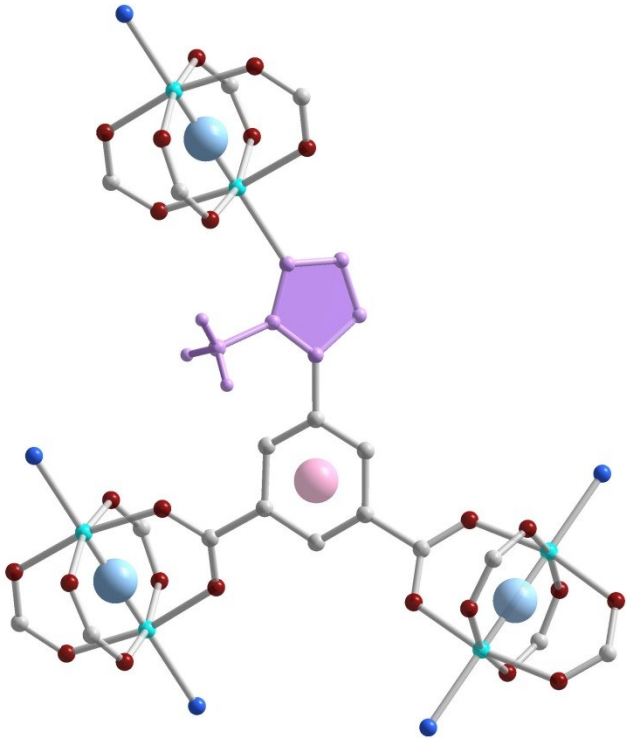

Fig. S7 View of ligand connection in **NTU-12**.

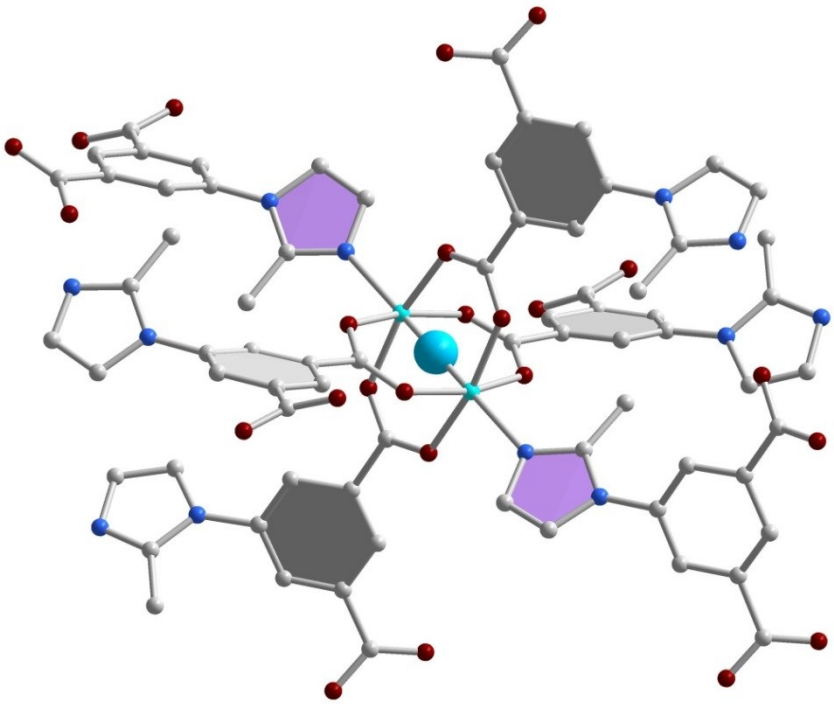

Fig. S8 View of cluster connection in **NTU-12**.

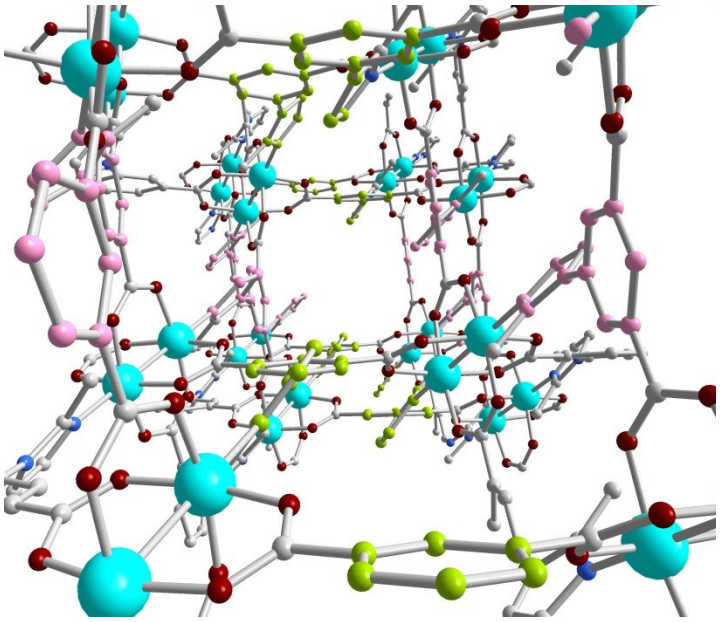

Fig. S9 View of 1D channel in **NTU-12** along c-axis.

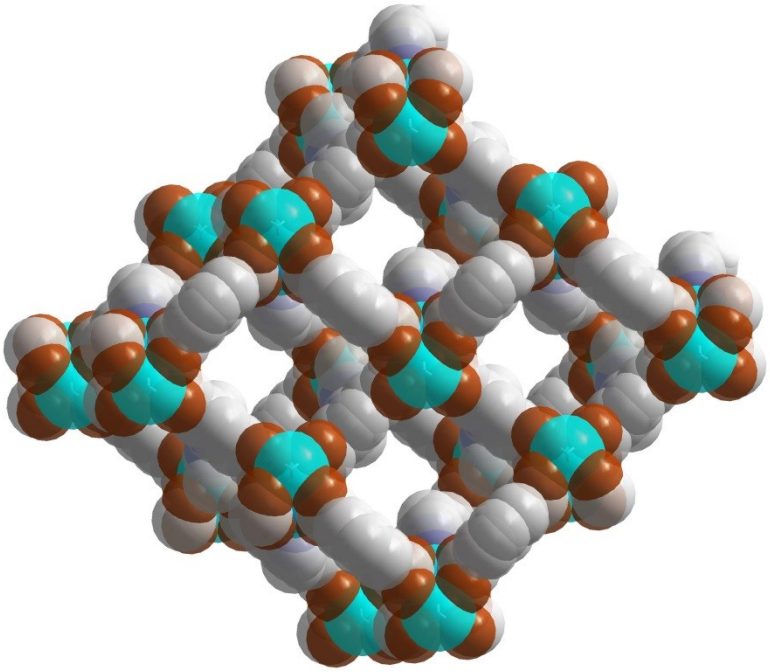

Fig. S10 View of crystal packing along c-axis in **NTU-12**.

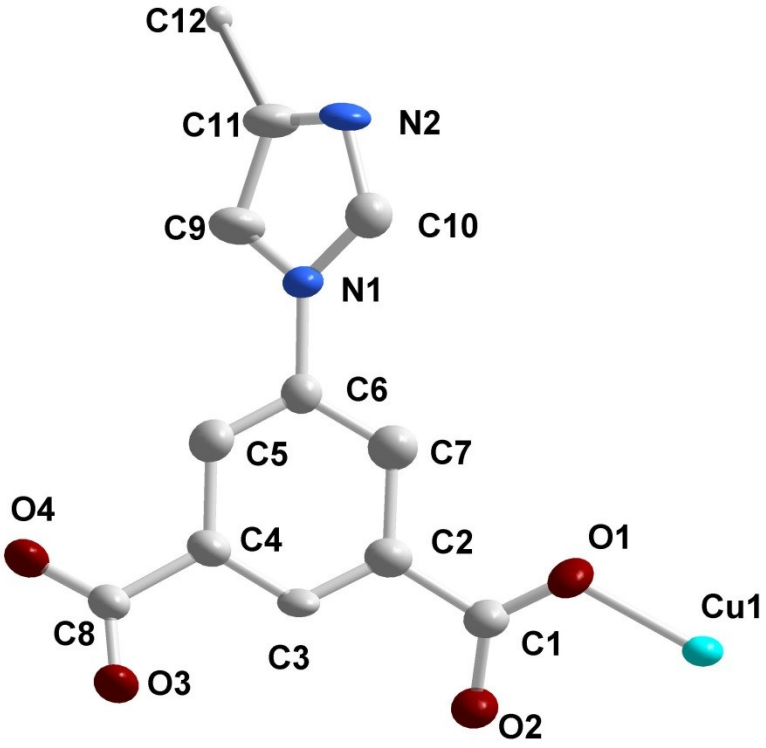

Fig. S11 View of asymmetric unit of **NTU-13**.

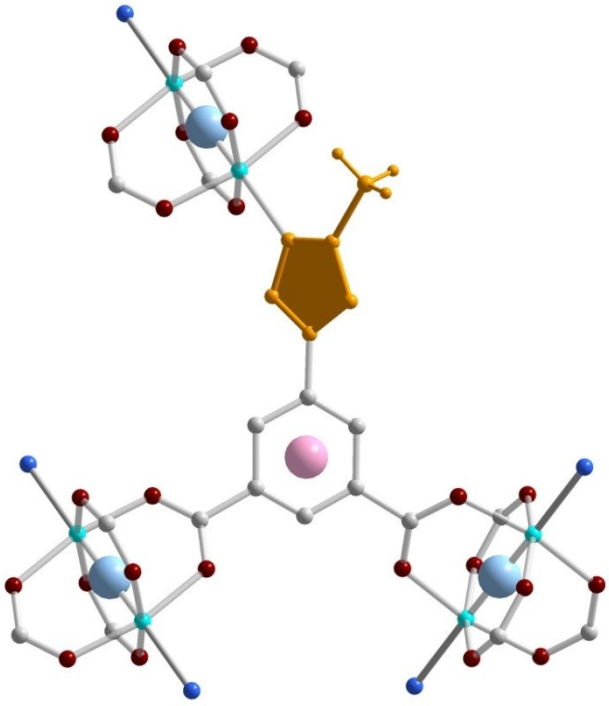

Fig. S12 View of ligand connection in **NTU-13**.

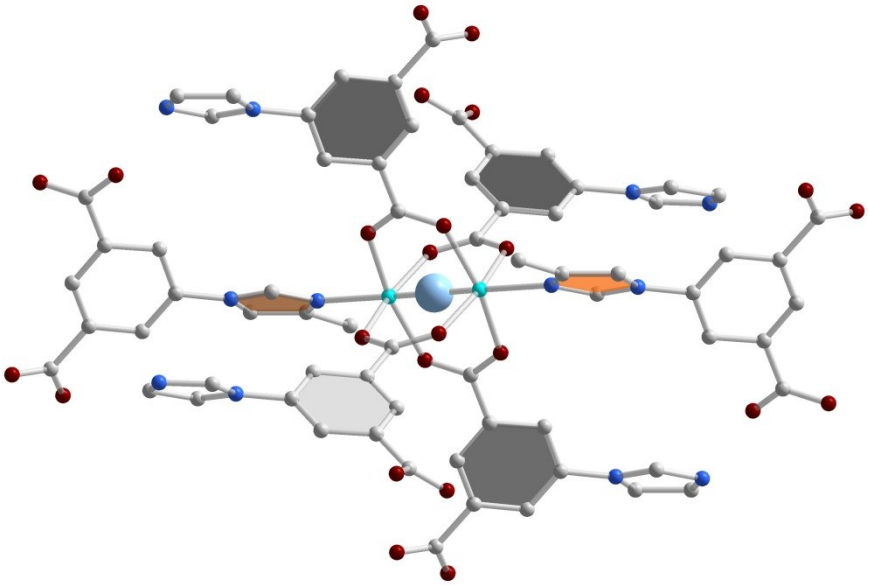

Fig. S13 View of cluster connection in **NTU-13**.

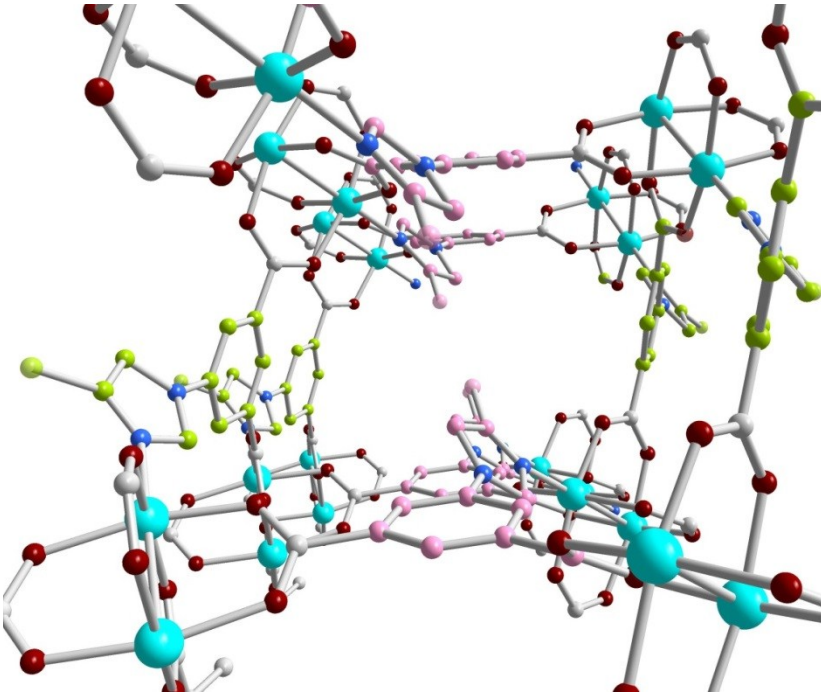

Fig. S14 View of 1D channel in **NTU-13** along c-axis.

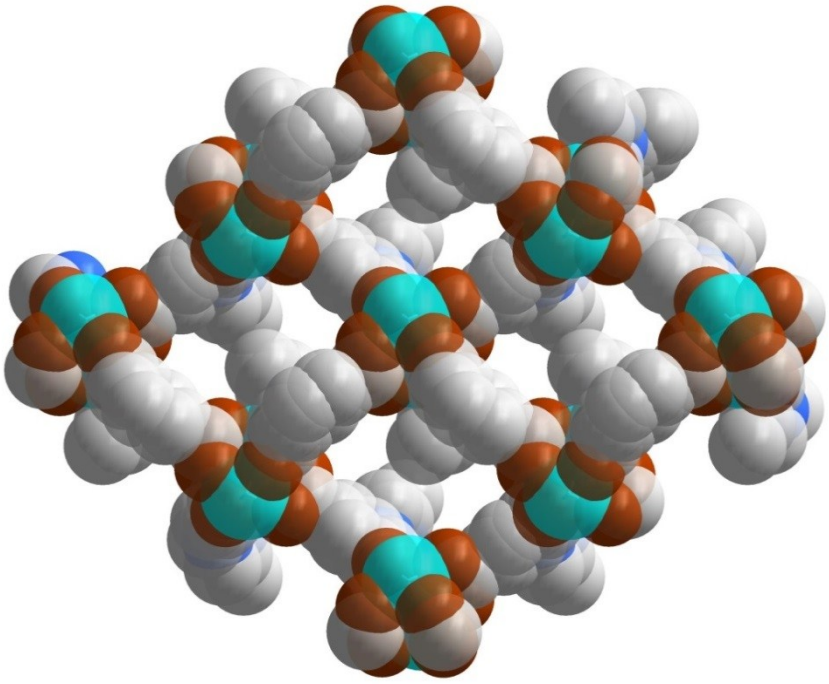

Fig. S15 View of crystal packing along c-axis in **NTU-13**.

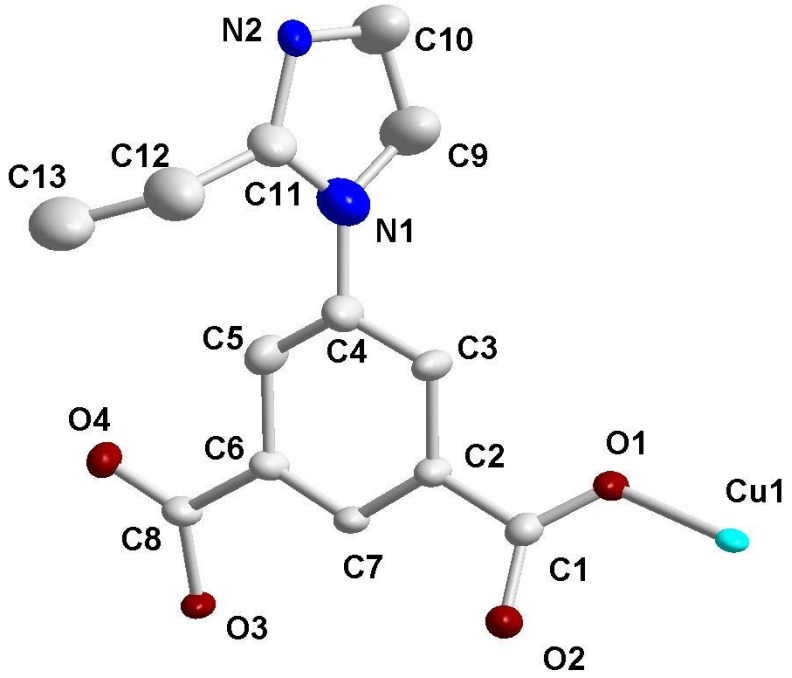

Fig. S16 View of asymmetric unit of **NTU-14**.

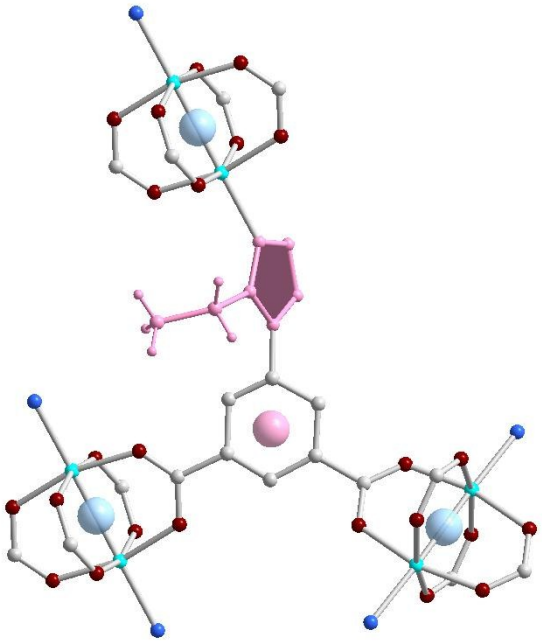

Fig. S17 View of ligand connection in **NTU-14**.

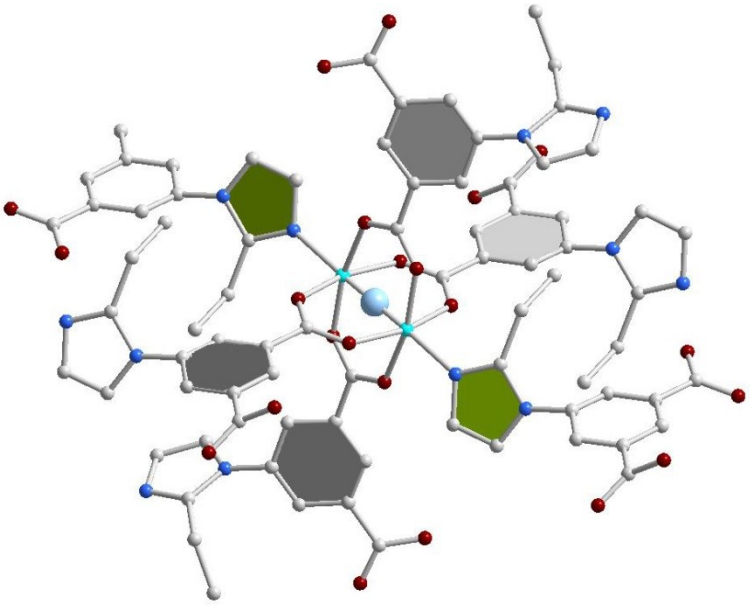

Fig. S18 View of cluster connection in **NTU-14**.

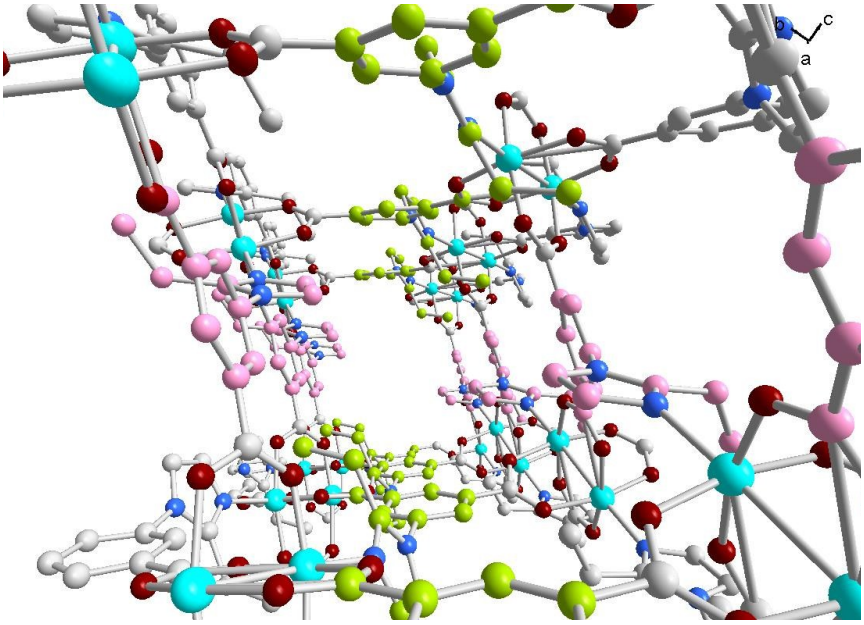

Fig. S19 View of 1D channel in **NTU-14** along c-axis.

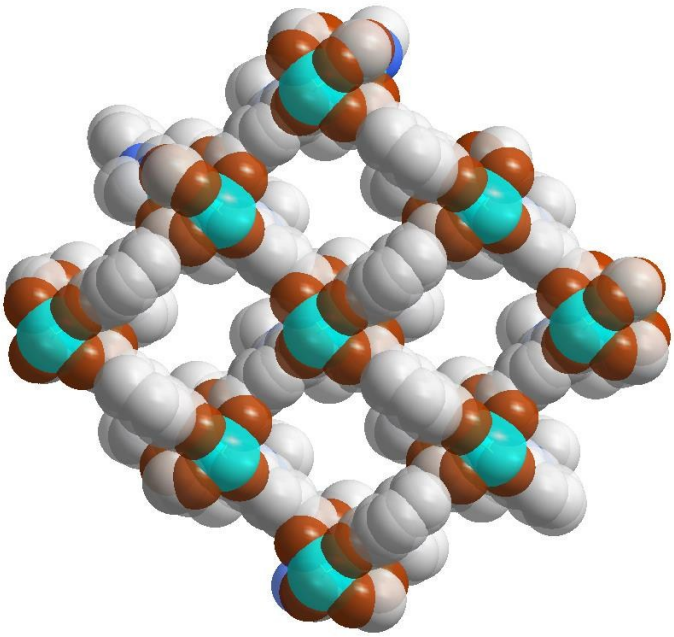

Fig. S20 View of crystal packing along c-axis in **NTU-14**.

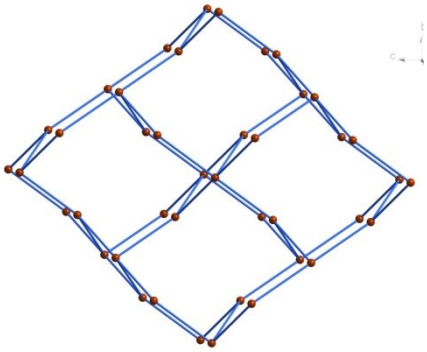

3,6-c apo/alpha topology of **NTU-11**

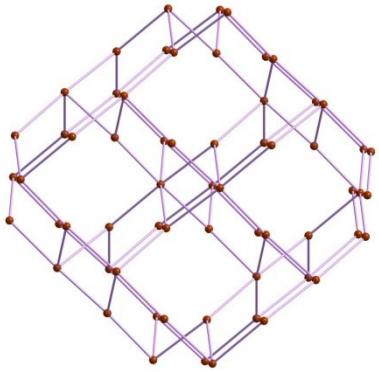

3,6-c apo/alpha topology of **NTU-12**

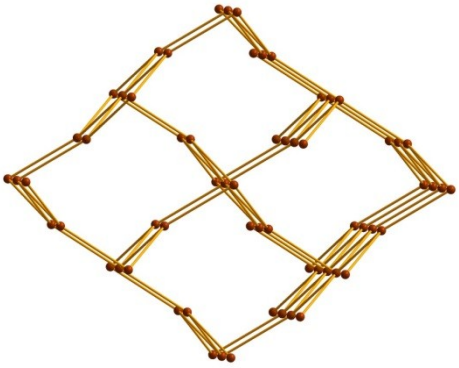

3,6-c apo/alpha topology of **NTU-13**

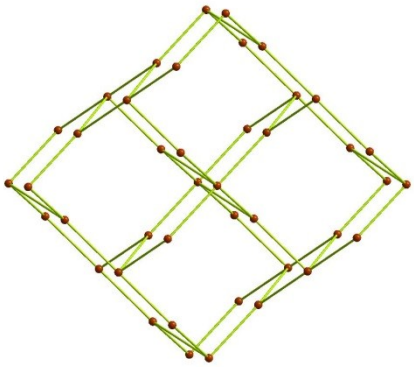

3,6-c apo/alpha topology of **NTU-14**

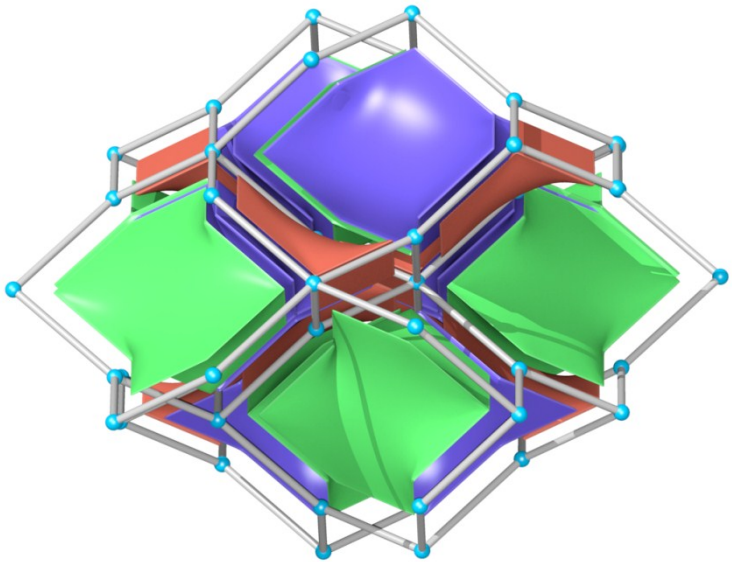

Tiles of apo/alpha net

Fig. S21 Topology comparison and tiles of **NTU-11** to **-14**.

Structural characterizations

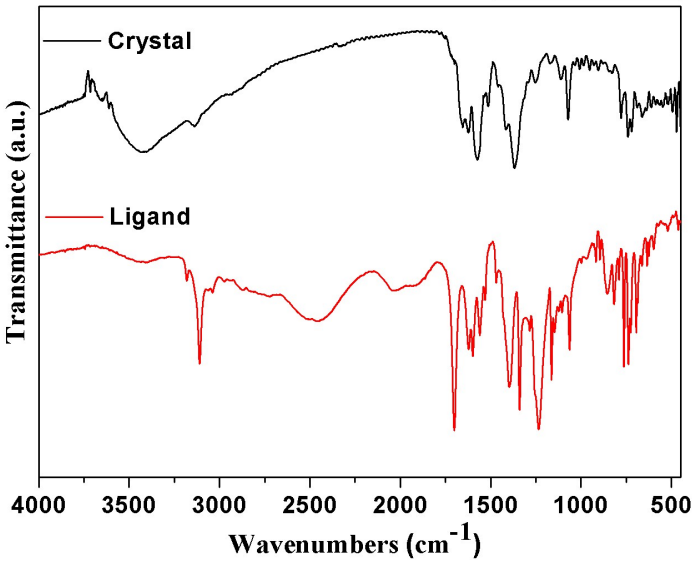

Fig. S22 IR of as-synthesized crystal of **NTU-11** and **H_3L^1** ligand.

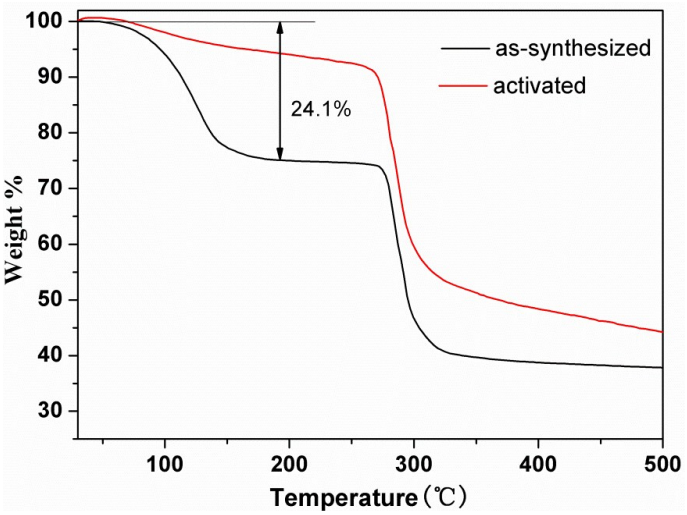

Fig. S23 TG of as-synthesized and activated **NTU-11**. The weight loss before 100 °C of activated sample should be assigned as the quick moisture adsorption in air during sample loading. Combine the squeezed electronic, the solvent inside the channel can be evaluated. The electronic number of H_2O is 10, while the electronic number of DMF is 40. Therefore: Number of electronics: (10+40) × 4 = 200 (found: 197); TG weight loss: (18+73)/[(18+73)+293.7] = 23.6% (found: 24.1%).

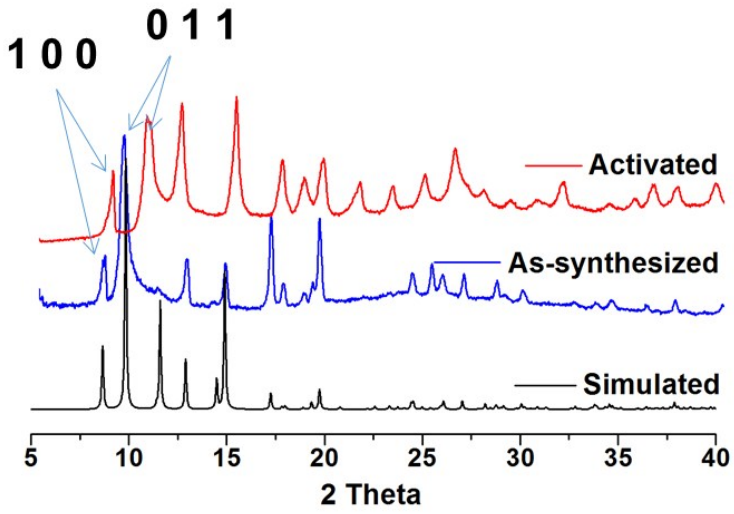

Fig. S24 PXRD of simulated and as-synthesized **NTU-11**.

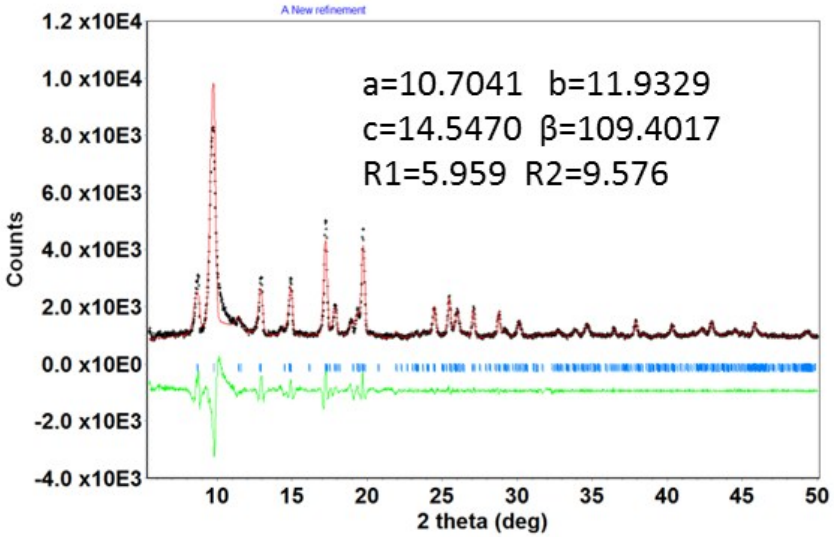

Fig. S25 The results of Le Bail analysis for the PXRD of **NTU-11**. Refined parameters and reliability factors are close to the data that derived from single crystal analysis.

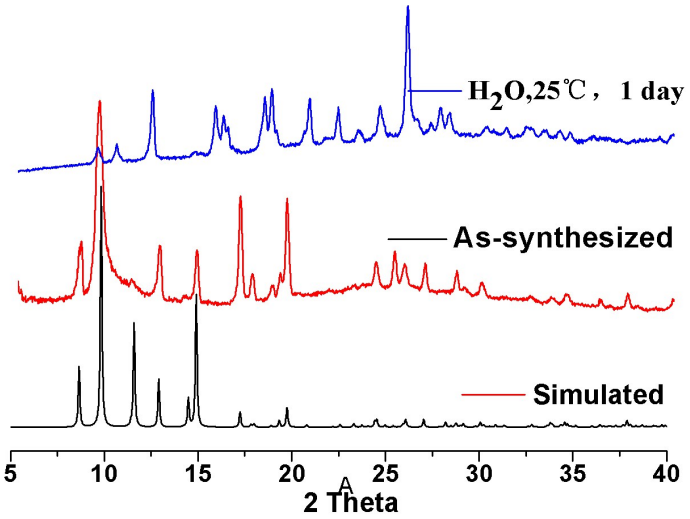

Fig. S26 PXRD results of water treated and fresh crystal of **NTU-11**. Shifted position of some peaks indicates weak water stability.

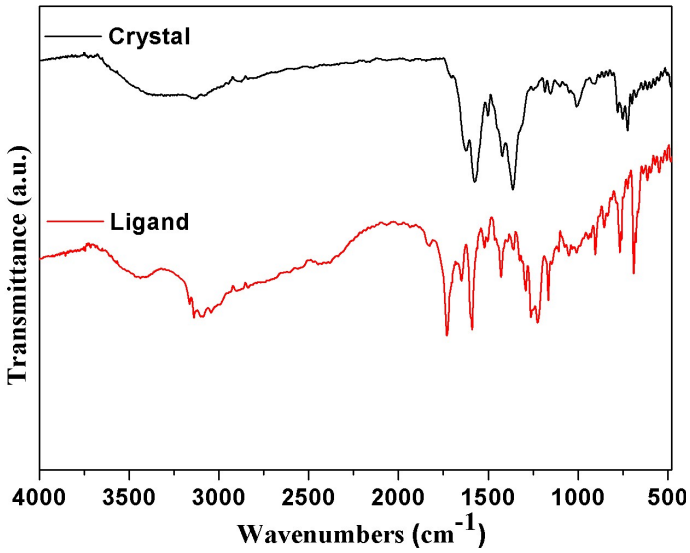

Fig. S27 IR of as-synthesized **NTU-12** and **H_3L^2** ligand.

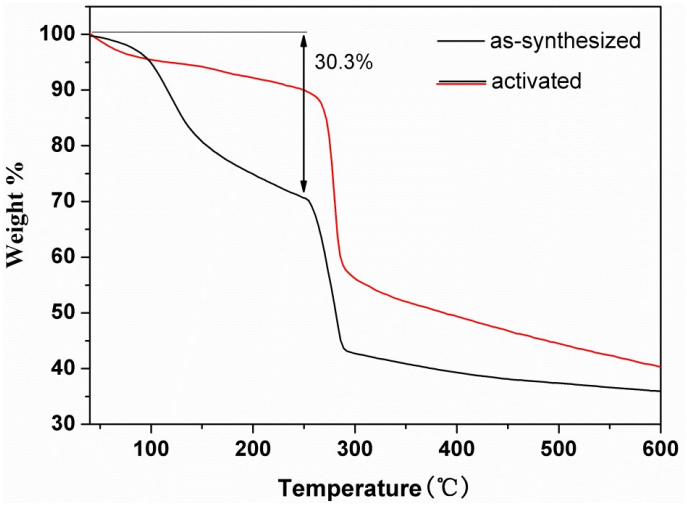

Fig. S28 TG of as-synthesized and activated **NTU-12**. The weight loss before 100 °C of activated sample should be assigned as the quick moisture adsorption in air during sample loading. Combine the squeezed electronic, the solvent inside the channel can be evaluated. The electronic number of H_2O is 10, while the electronic number of DMF is 40. Therefore: Number of electronics: (10×1.5+40×1.5) × 8 = 600 (found: 609); TG weight loss: (1.5×18+1.5×73)/ [(1.5×18+1.5×73)+307.75] = 30.7% (found: 30.3%).

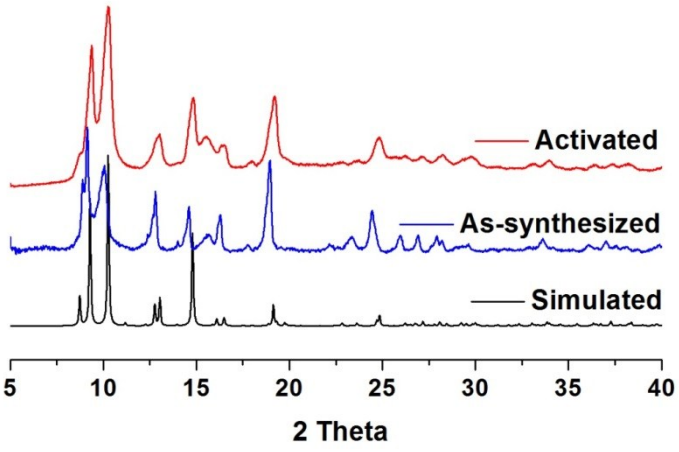

Fig. S29 PXRD of simulated, as-synthesized and activated **NTU-12**.

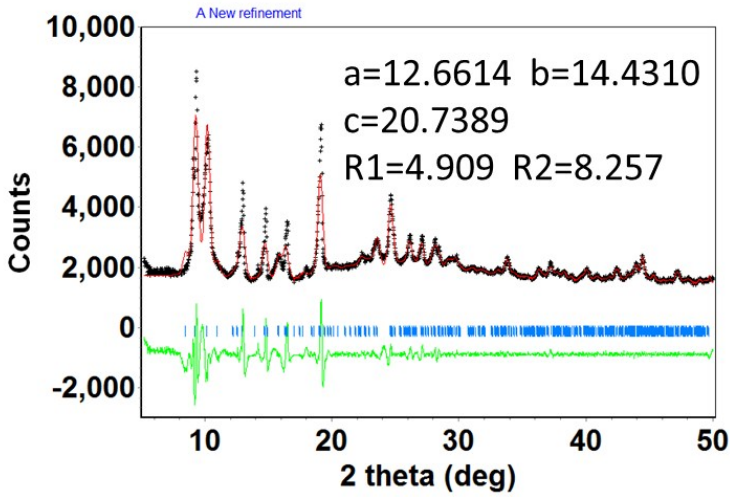

Fig. S30 The results of Le Bail analysis for the PXRD of **NTU-12**. Refined parameters and reliability factors are close to the data that derived from single crystal analysis.

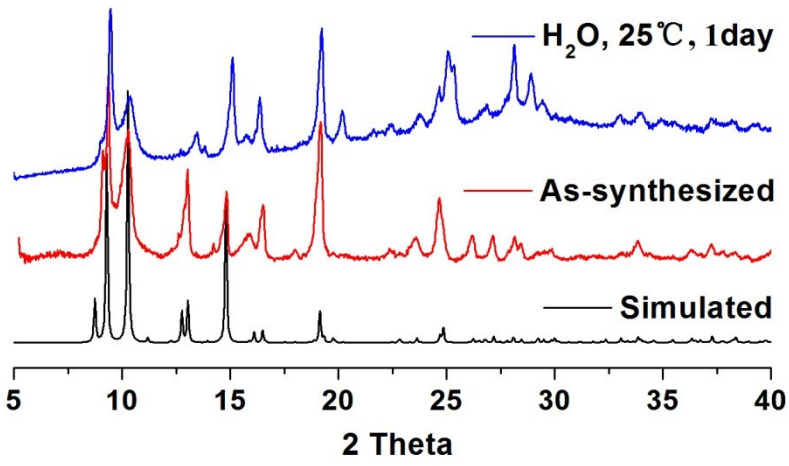

Fig. S31 PXRD results of water treated and fresh crystal of **NTU-12**.

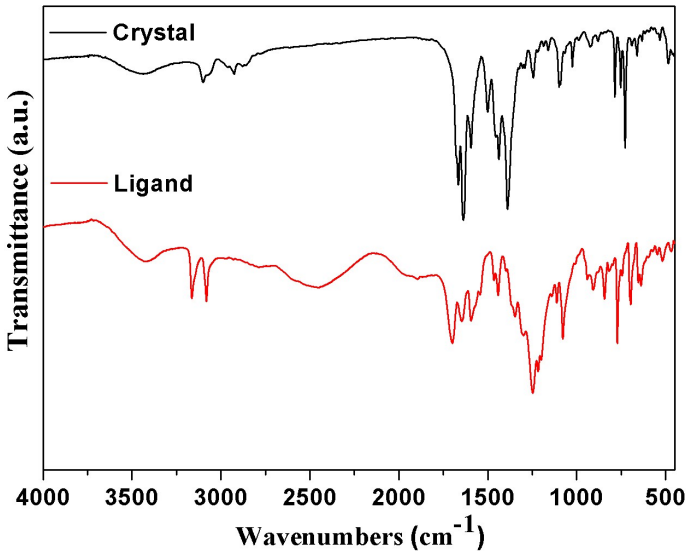

Fig. S32 IR of as-synthesized crystal of **NTU-13** and **H_3L^3** ligand.

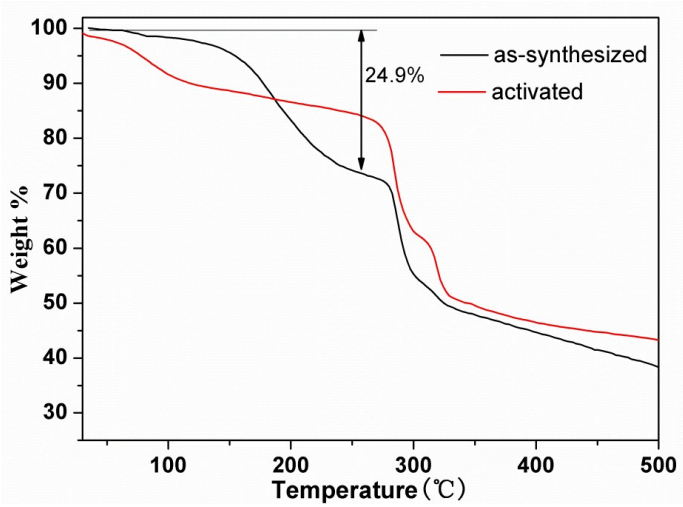

Fig. S33 TG of as-synthesized and activated **NTU-13**. The weight loss before 100 °C of activated sample should be assigned as the quick moisture adsorption in air during sample loading. ombine the squeezed electronic, the solvent inside the channel can be evaluated. The electronic number of H_2O is 10, while the electronic number of DMF is 40. Therefore: Number of electronics: (10×1.5+40) × 4 = 220 (found: 221); TG weight loss: (1.5×18+73)/[(1.5×18+73)+307.7] = 24.5% (found: 24.9%).

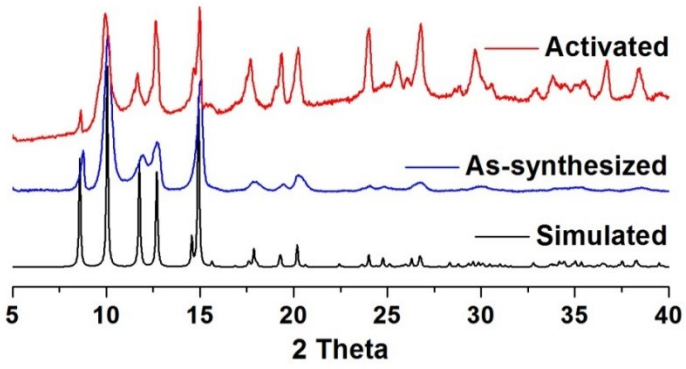

Fig. S34 PXRD of simulated, as-synthesized and activated **NTU-13**.

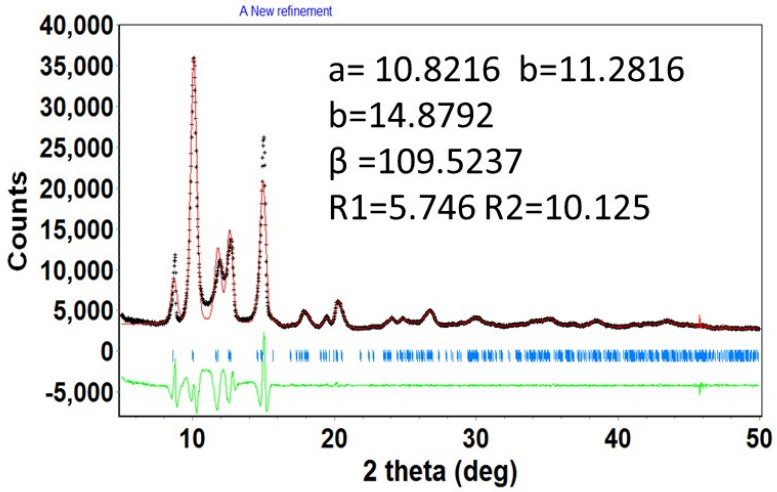

Fig. S35 The results of Le Bail analysis for the PXRD of **NTU-13**. Refined parameters and reliability factors are close to the data that derived from single crystal analysis.

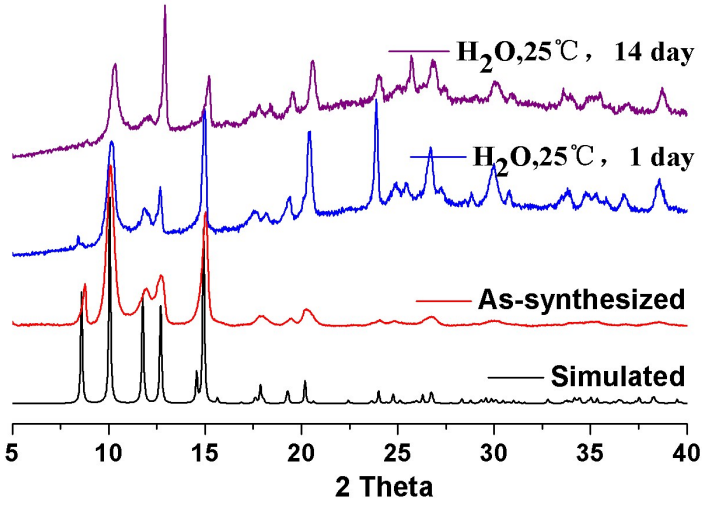

Fig. S36 PXRD results of water treated and fresh crystal of **NTU-13**.

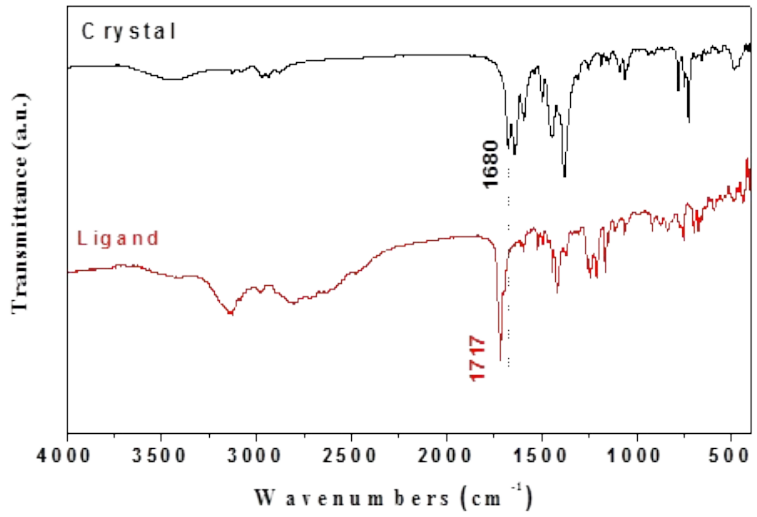

Fig. S37 IR of as-synthesized crystal of **NTU-14** and **H_3L^4** ligand.

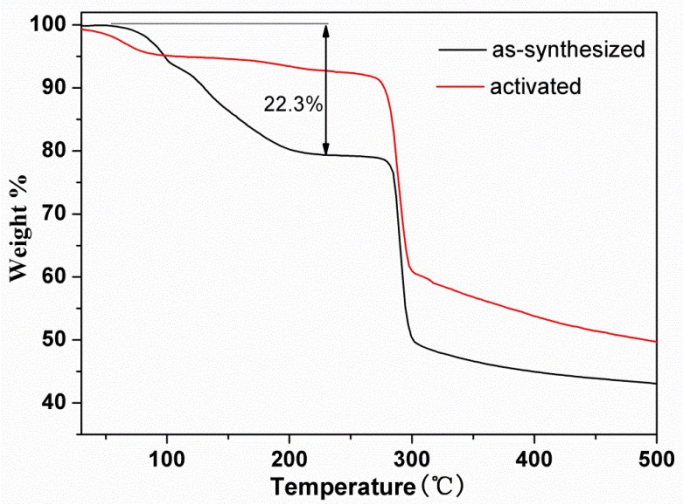

Fig. S38 TG of as-synthesized and activated **NTU-14**. The weight loss before 80 °C of activated sample should be assigned as the quick moisture adsorption in air during sample loading. Combine the squeezed electronic, the solvent inside the channel can be evaluated. The electronic number of H_2O is 10, while the electronic number of DMF is 40. Therefore: Number of electronics: (10×1.2+40) × 4 = 210 (found: 209); TG weight loss: (1.2×18+73)/ [(1.2×18+73)+321.7] = 22.7% (found: 22.3%).

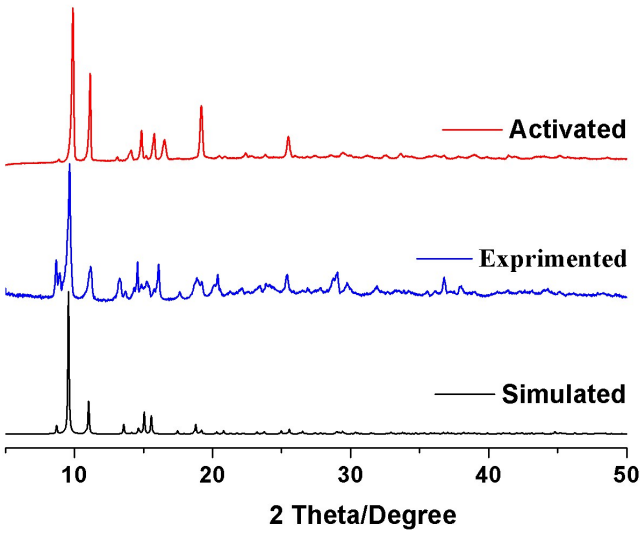

Fig. S39 PXRD of simulated, as-synthesized and activated **NTU-14**.

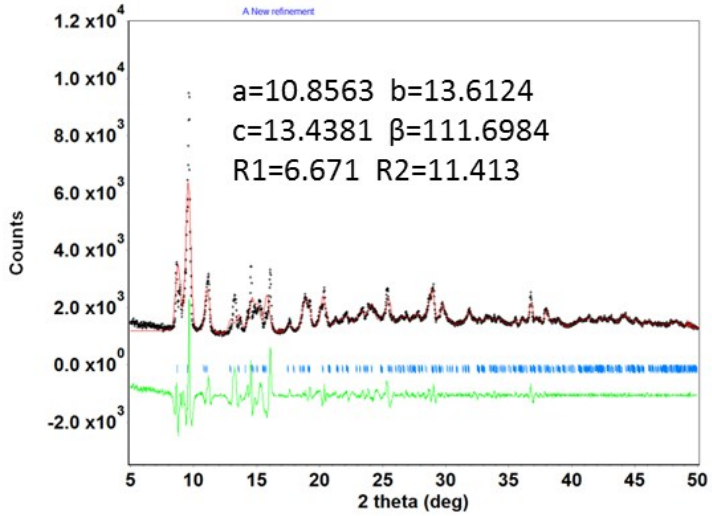

Fig. S40 The results of Le Bail analysis for the PXRD of **NTU-14**. Refined parameters and reliability factors are close to the data that derived from single crystal analysis.

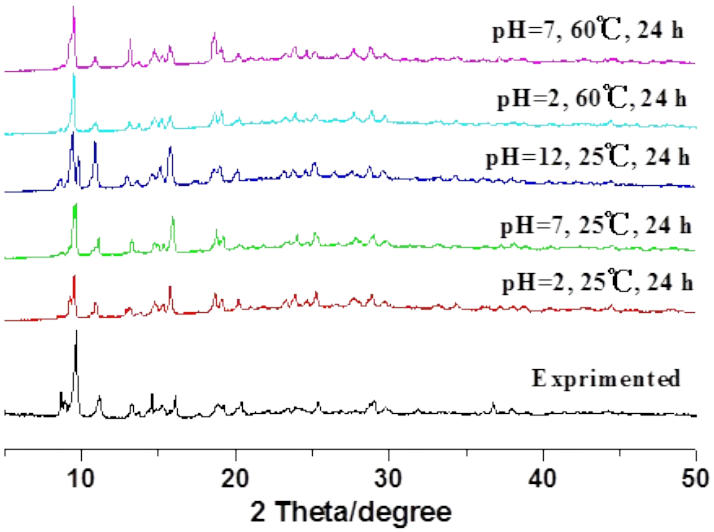

Fig. S41 PXRD of water and chemical treated **NTU-14**.

Adsorption isotherms

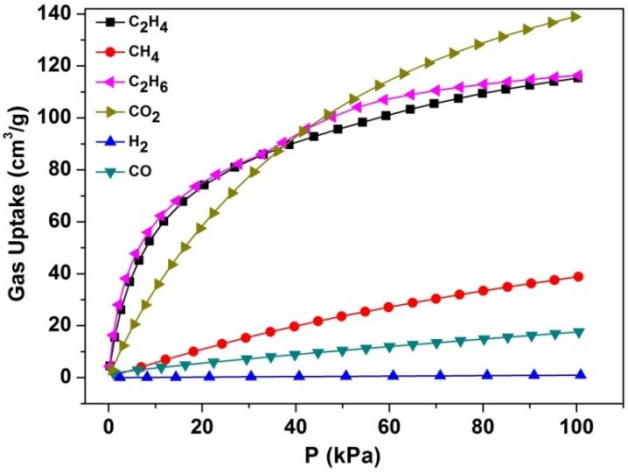

Fig. S42 Gas adsorption of **NTU-12** at 273 K.

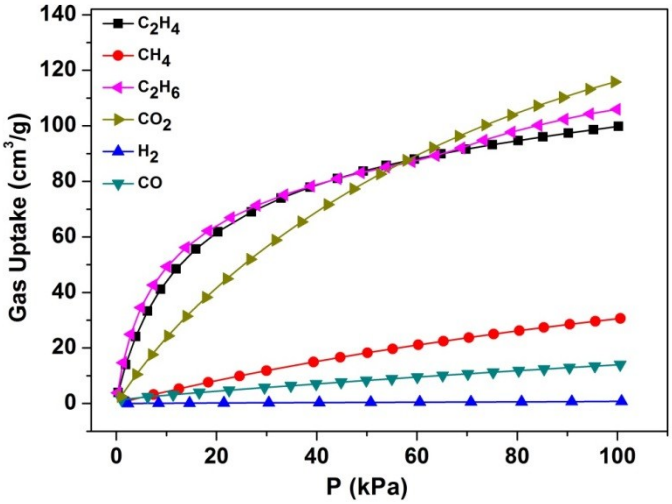

Fig. S43 Gas adsorption of **NTU-12** at 283 K.

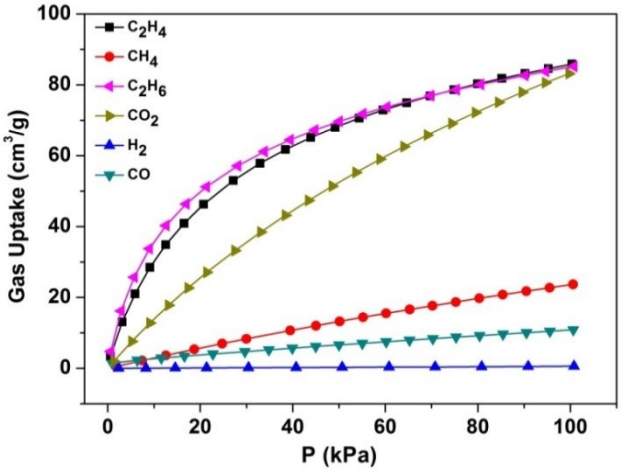

Fig. S44 Gas adsorption of **NTU-12** at 298 K.

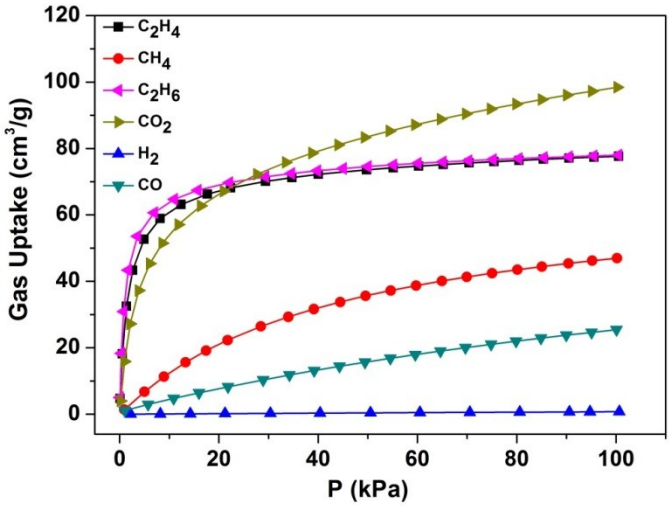

Fig. S45 Gas adsorption of **NTU-13** at 273 K.

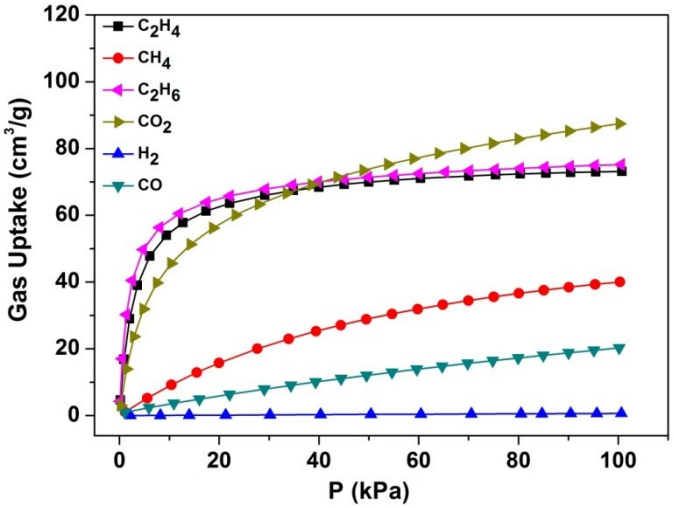

Fig. S46 Gas adsorption of **NTU-13** at 283 K.

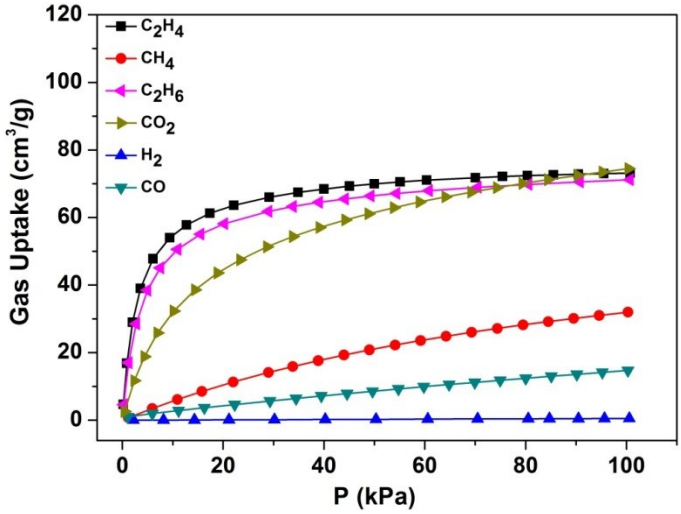

Fig. S47 Gas adsorption of **NTU-13** at 298 K.

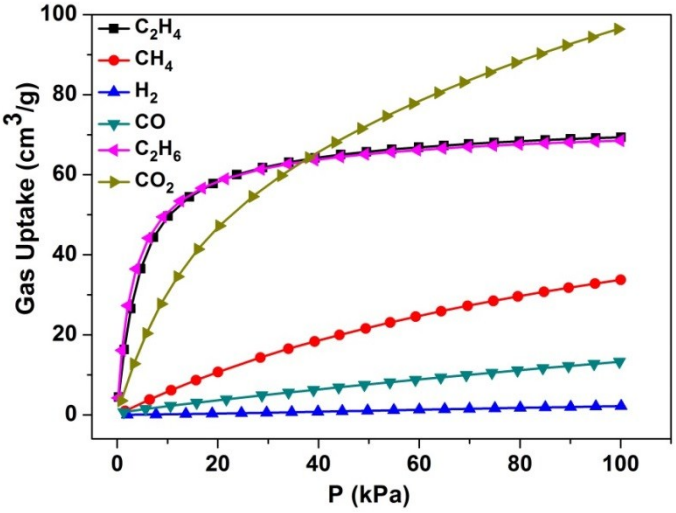

Fig. S48 Gas adsorption of **NTU-14** at 273 K.

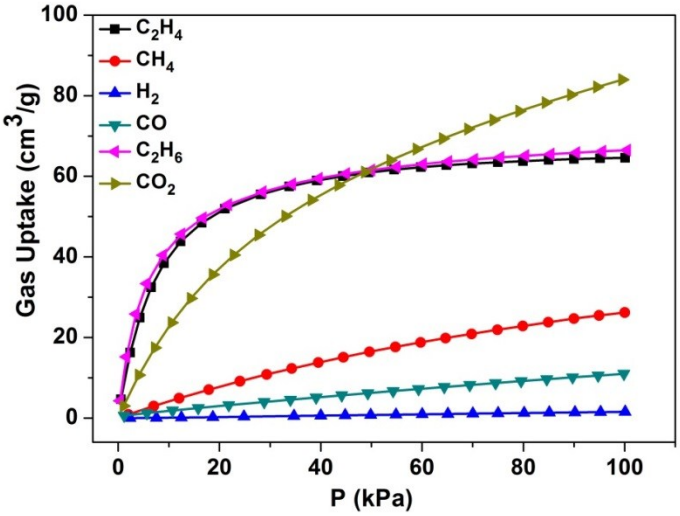

Fig. S49 Gas adsorption of **NTU-14** at 283 K.

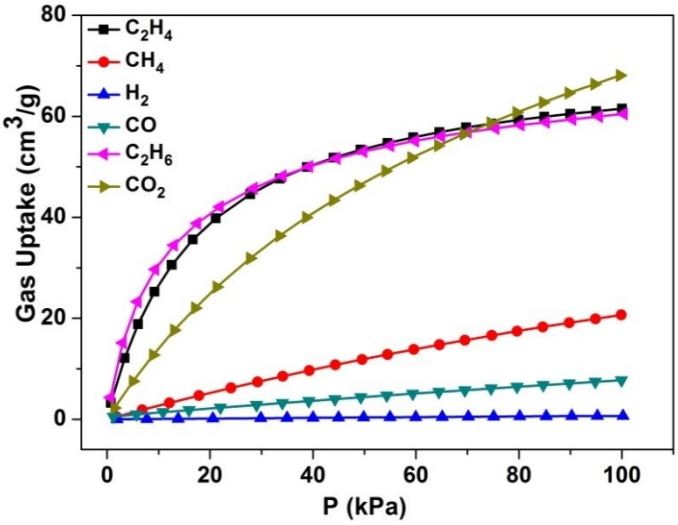

Fig. S50 Gas adsorption of **NTU-14** at 298 K.

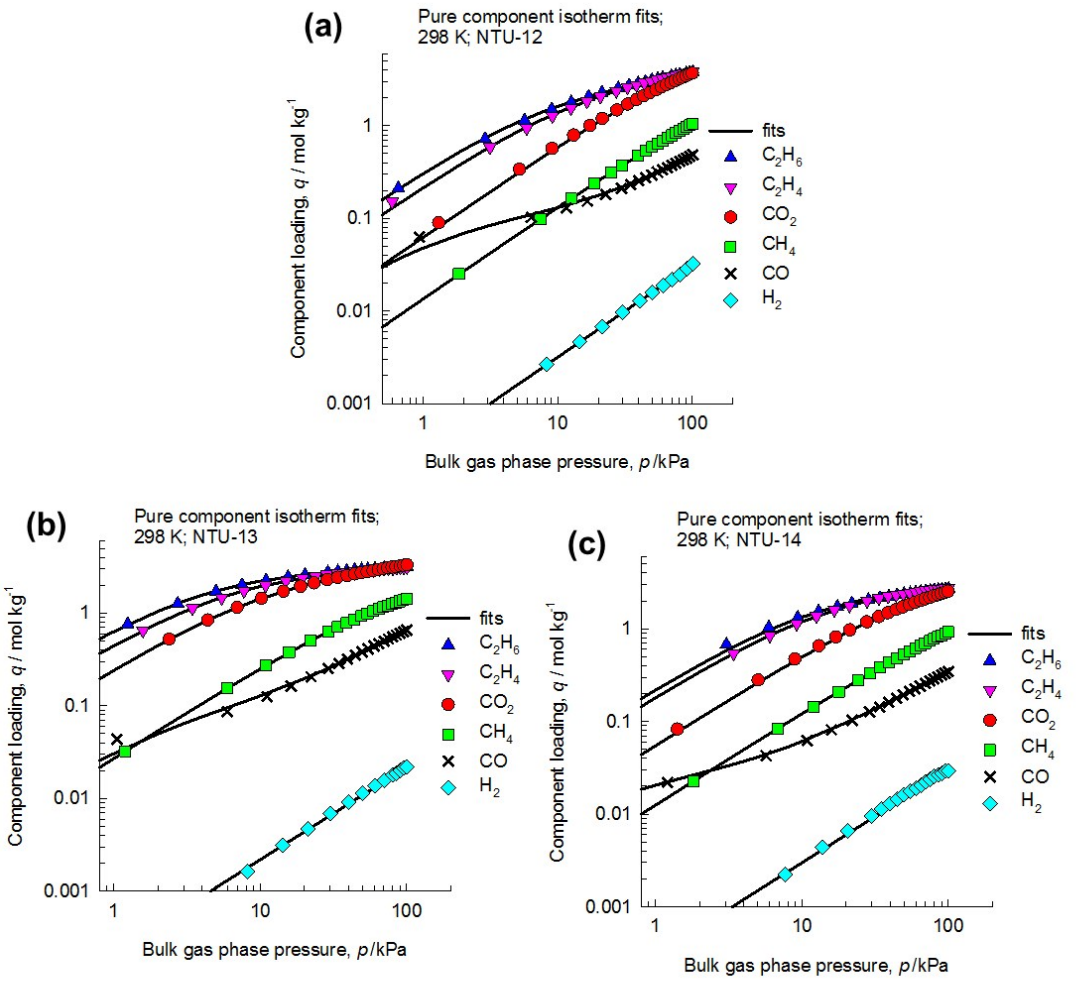

Fig. S51 Comparison of experimental data on component loadings for H_2, CH_4, CO, CO_2, C_2H_4, and C_2H_6 at 298 K in (a) **NTU-12**, (b) **NTU-13**, and (c) **NTU-14** at 298 K with the isotherm fits.

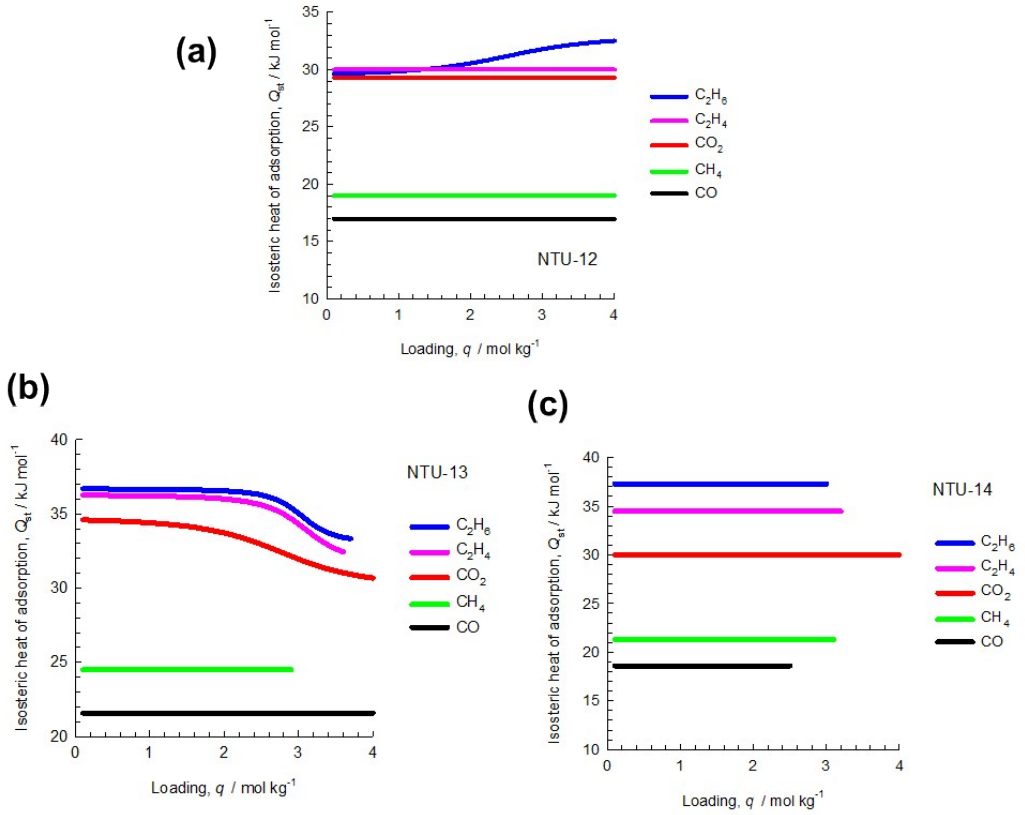

Fig. S52 The isosteric heat of adsorption, Q_{st}, for CH_4, CO, CO_2, C_2H_4, and C_2H_6 at 298 K in (a) **NTU-12**, (b) **NTU-13**, and (c) **NTU-14** at 298 K**.** The determination of the Q_{st} is based on the Clausius-Clapeyron equation.

Table S6. Calculated gas selectivity in **NTU-12**, **-13** and **-14** by IAST model at 298K, 1bar.

	C_2H_4/CH_4	CO_2/CH_4	C_2H_4/CO	CO_2/CO	C_2H_4/H_2
NTU-12	14.7	5.6	40.3	13.2	688.8
NTU-13	20.4	10.5	44.4	26.3	1391.8
NTU-14	15.2	6.9	60.9	23.8	472.5

From this table, we note that the selectivity of CO_2/CO in **NTU-12** (13.2) was improved 2 times in **NTU-13** (26.29) and 1.8 times in **NTU-14** (23.8). In addition, the selectivity of C_2H_4/CH_4 also shows obvious improvement in **NTU-13** (20.4) and **-14** (15.2), indicating high practical feasibility of C1/C2 hydrocarbon separation. Meanwhile, due to low H_2 uptake, the C_2H_4/H_2 selectivity in them was predicted to be extremely high. Therefore, the inherent gas selectivities for those three PCPs appear to be dictated by host-guest interactions, and also polarizability of molecules.

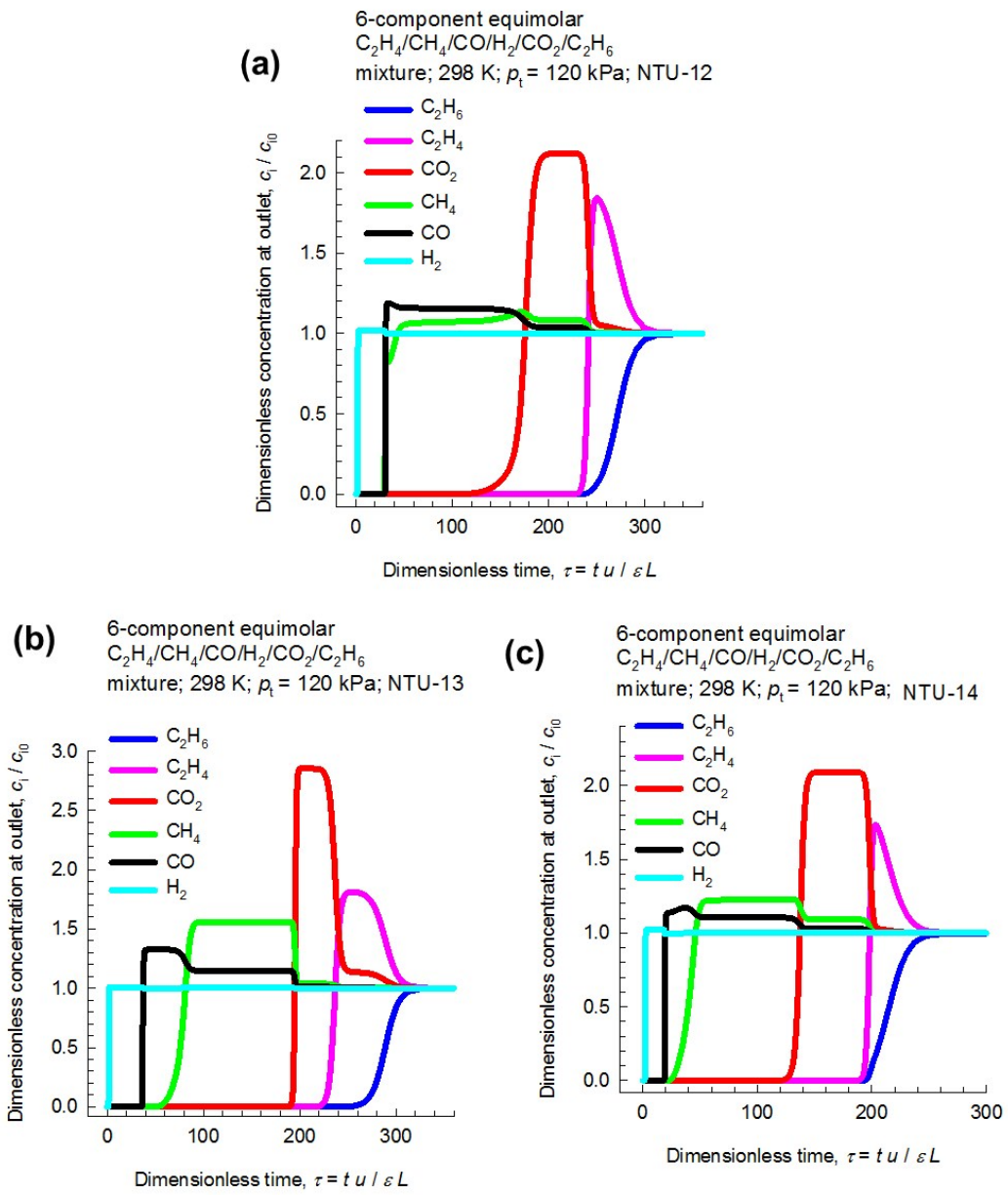

Fig. S53 Transient breakthrough simulations for separation of equimolar 6-component mixtures containing H_2, CH_4, CO, CO_2, C_2H_4, and C_2H_6 at 298 K using (a) **NTU-12**, (b) **NTU-13**, and (c) **NTU-14** at 298 K. The total inlet pressure is 120 kPa, with partial pressures of 20 kPa each.

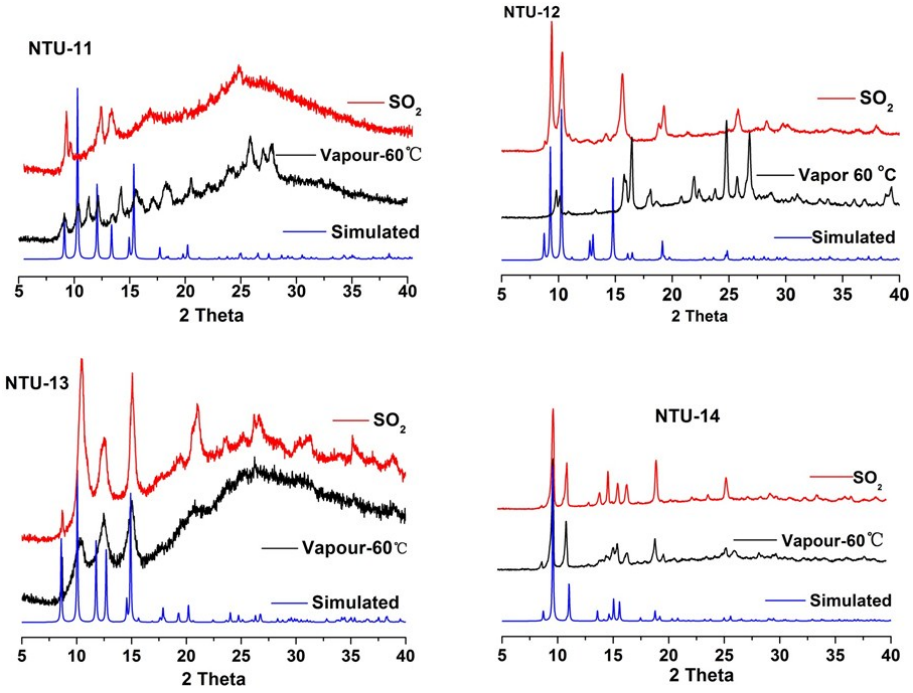

Fig. S54 PXRD of water vapor and SO_2 treated NTU-11 to -14. Fully activated PCPs were treated by water vapor (60℃) or SO_2 (25℃) for 24 h, respectively.

Membrane preparation

The **NTU-14** particles were dispersed in a solvent mixture of 70 wt % ethanol and 30 wt % water and then treated by ultrasonication and stirring for 1/2 h for three times each. The crystals were first ‘‘primed’’ by adding a certain amount of PEBA polymer and stirred for another 2 h at 80 ^{o}C (w PEBA: w EtOH/H_2O=1 : 100). Subsequently, the suspension containing primed particles was mixed with the remaining bulk polymer (w PEBA : w EtOH/H_2O = 4 : 100) and kept on stirring for another 2 h. After that, the solution kept at 60 ^{o}C overnight to eliminate trapped air bubbles. The hybrid composite membranes were cast on PVDF substrate using spin-coating method. Following removal of the solvent under room temperature for 24 h and then curing in the oven at 70 ^{o}C for 12 h, the **NTU-14** filled PEBA membrane was fabricated. Similarly using the PEBA solution (5 wt%) without mixed with NTU-14 particles, the unfilled PEBA membrane was prepared as described above. The loading in the membrane was calculated as following formula:

$$w_{PCP} = \frac{m_{PCP}}{m_{CS}} \times 100\% \quad (1)$$

where w_{MOF} is the particle loading, m_{MOF} and m_{PEBA} represent the weights of **NTU-14** and PEBA, respectively. The loading of these membranes in present study was 4 wt%.

Membrane Characterization

Gas transport performances were measured by gas permeation test using constant pressure/variable volume technique. For pure gas permeation tests of CO_2 and CH_4, the condition was set as 0.3 MPa at room temperature. After the system reached steady-state, all the gas permeation measurements were performed more than three times, and the gas permeance was calculated using the following equation:

$$P = \frac{Q}{\Delta PA}$$

where P is the gas permeance [1 GPU= 10^{-10} cm^3 (STP) /(cm^2 s cmHg)], Q is the volume permeate rate of gas (cm^3/s) at standard temperature and pressure (STP), ΔP is the transmembrane pressure (cmHg) and A is the effective membrane area (2.27 cm^2 in this work). The ideal selectivity of CO_2/CH_4 can be calculated by the ratio of the permeability of the individual gas which can be expressed as follows:

$$\alpha = \frac{P_A}{P_B}$$

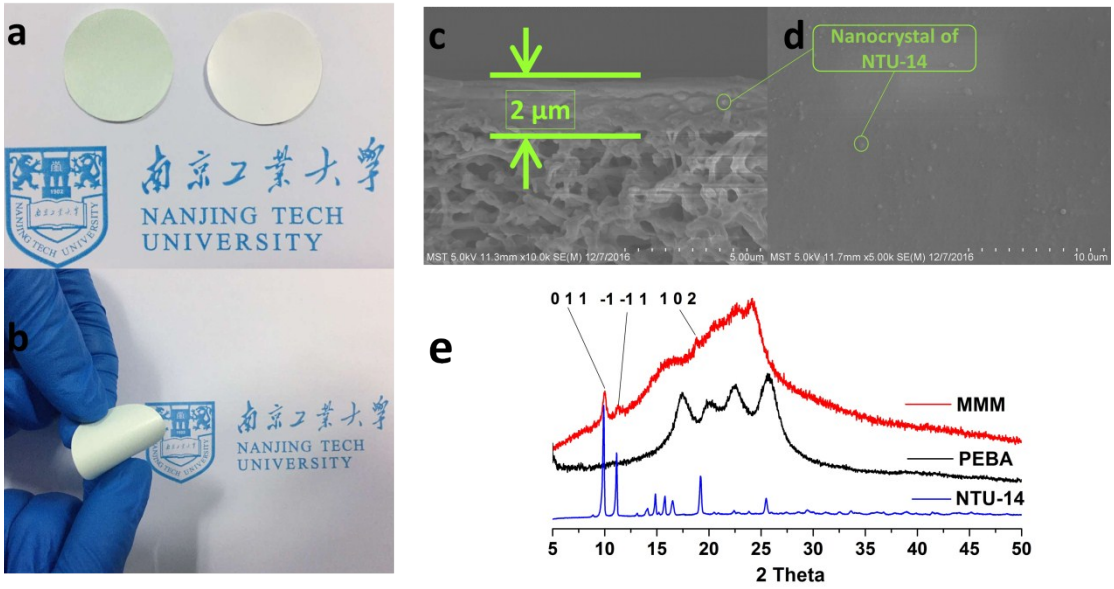

Fig. S55 Photo image of **NTU-14** MMM and pure PEBA membrane (a); flexibility of **NTU-14** MMM (b); SEM image of cross section of **NTU-14** MMM (c); SEM image of top view of **NTU-14** MMM (d); PXRD of **NTU-14** MMM (e).

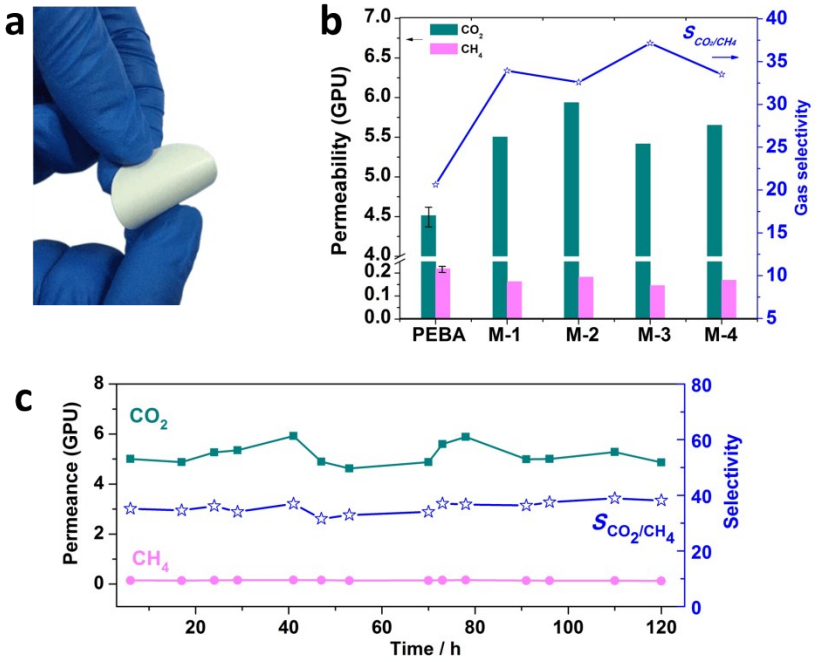

Fig. S56 View of flexible NTU-14/PEBA with light green colour (a), comparison of gas selectivity in PEBA and three MMMs (b), long term working of **NTU-14** MMM at room temperature (c).

Notation

b	Langmuir constant, Pa^{-1}
L	length of packed bed adsorber, m
p_i	partial pressure of species *i* in mixture, Pa
p_t	total system pressure, Pa
q_i	component molar loading of species *i*, mol kg^{-1}
q_t	total molar loading in mixture, mol kg^{-1}
q_{sat}	saturation loading, mol kg^{-1}
R	gas constant, 8.314 J mol^{-1} K^{-1}
t	time, s
T	absolute temperature, K
u	superficial gas velocity in packed bed, m s^{-1}
z	distance along the adsorber, and along membrane layer, m

Greek letters

□	voidage of packed bed, dimensionless
□	framework density, kg m^{-3}
□	time, dimensionless

Subscripts

i	referring to component *i*
t	referring to total mixture

Refs:

1 Sheldrick, G. M. A short history of SHELX. *Acta Crystallogr. Sec. A* **64**, 112-122, (2008).

2 Vandersluis, P. & Spek, A. L. Bypass - an Effective Method for the Refinement of Crystal-Structures Containing Disordered Solvent Regions. *Acta Crystallogr. Sec. A* **46**, 194-201, (1990).

3 Spek, A. L. Single-crystal structure validation with the program PLATON. *J. Appl. Crystallogr.* **36**, 7-13, (2003).

4 Krishna, R. The Maxwell-Stefan description of mixture diffusion in nanoporous crystalline materials. *Microporous Mesoporous Mater.* **185**, 30-50, (2014).

5 Krishna, R. Methodologies for evaluation of metal-organic frameworks in separation applications. *Rsc Adv* **5**, 52269-52295, (2015).

6 Krishna, R. Methodologies for Evaluation of Metal-Organic Frameworks in Separation Applications. *RSC Advances* **5**, 52269-52295, (2015).